行政院國家科學委員會專題研究計畫 期末報告

以光場增強效應提升薄膜太陽能電池吸收效率研究

計 畫 類 別 ：個別型
計 畫 編 號 ：NSC 101-2218-E-009-001-
執 行 期 間 ：101 年 03 月 01 日至 102 年 09 月 30 日
執 行 單 位 ：國立交通大學電子工程學系及電子研究所

計 畫 主 持 人：林詩淳

報 告 附 件 ：出席國際會議研究心得報告及發表論文

公 開 資 訊 ：本計畫可公開查詢

中 華 民 國 102 年 12 月 18 日

中 文 摘 要 ： 本研究計畫主要是針對光電太陽能元件的光學特性之基礎研究，其成果包括三個研究方向：（一）(一)利用周期性寬頻高效率光場增強陣列光子晶體，提出新式太陽能電池結構，並將光譜分離式共振腔結構應用於多接面太陽能電池上(high-efficiency resonant-cavity-like structures for multi-junction or multi-band solar cell application)。相對於隨機幾何繞射結構，周期性的結構可提供可重複且較穩定的效率轉換。在這一次的計畫之中，我們運用了表面電漿子陣列(surface plasmon array)，來提供光場增強的效應，透過在薄膜太陽能電池的上下兩端的表面電漿子陣列。我們形成了一個共振腔結構，進而達到相當良好的光場增強效應和效率提升。(二) 本計畫之第二個研究方向，為進行光學特性的基礎研究，以增進對太陽能電池中，光場增強效應(Light Trapping) 之深入了解。這一個研究之重點 在於計算太陽能電池之光學特徵模式(eigen mode)。在了解了特徵模式之後，在進一步研究導膜共振(guided mode resonance)之形成，和如何增強此一共振並達到寬頻增益。(三) 進行隨機幾何形狀應用於太陽能電池底部反射鏡(back reflector) 之研究，將利用基因演算法來進行幾何形狀之最佳化，決定最適合運用在太陽能電池的幾何形狀。在這一次的計畫中，最佳化之隨機幾何底部反射鏡的效率，相比於週期性陣列，可以達到~30%之提升。

本計畫的執行得到了下面的成果：(I)前瞻光學共振腔型態元件的提案，將提供未來高效率太陽能電池的設計藍圖 (II)證實/示範運用奈米光學模擬可以有效的提升太陽能電池的設計，並透過有效的光場增強效應，太陽能電池的吸收與轉換效率可以得到顯著的提升，(III)透過特徵模式的分析、透射/反射/吸收頻譜的計算、和繞射級數的計算，提升對於太陽能電池基礎物理的了解，尤其是光子在元件中折射/反射/繞射的現象(IV)隨機幾何底部反射鏡之設計，將可以進一步提升薄膜矽太陽能電池的效率

中文關鍵詞： 太陽能電池 共振腔 隨機反射鏡 特徵模

英 文 摘 要 ： This research report is mainly for the fundamental research of photovoltaic device optics. The achievement can be separated into three parts (I) Cavity-resonant solar cells using subwavelength gratings, and application of cavity-resonant structure to multi-junction cells. The specific design in this study using plasmonic effect, which

can enhance the spectral splitting through surface plasonic subwavelength grating and therefore increase the photocurrent of multi-junction cells. (II) The second effort in this proposal is the fundamental understanding of light trapping phenomenon in photovoltaic cells. Specifically, the eigen mode and photonic bandstructure is studied, and their effect on the absorption enhancement is assessed. It should be noted that only through properly designed quasi-guided mode excitation, the thin-film solar cells can achieve their ultimate efficiency for a given active layer thickness. Other photonic enhancement approaches such as slow light and resonance enhancement are also preliminarily studied in this project. The last research effort of this project is (III) Improved randomized grating structures for high efficiency solar cells, through genetic algorithm optimization, and based on the physics studied in goal (II). The conventional randomly textured silver-dielectric back reflectors are widely used in commercial solar cells. Nonetheless, well-designed random structures have not been carefully examined and not been made possible. In this project, a lithographically definable random reflector is proposed, and its efficiency is shown to be ~30% higher than its periodic counterpart.
The success of this project contribute in (I)New/Novel/Promising optical cavity structures proposal provides directions for future high efficiency solar cell design. (II) Demonstration of using nano photonic modeling approach to design solar cell optical structures. (III) Improving the fundamental understanding of electrodynamic phenomenon inside solar cells by eigen mode analysis, transmission/reflection/absorption calculation, and diffraction order analysis. (IV) Design of randomized structures benefiting future high efficiency thin-film solar cells.

英文關鍵詞： solar cell, resonant cavity, randomized reflector, eigen mode

摘要

關鍵詞: 太陽能電池 共振腔　隨機反射鏡 特徵模

本研究計畫主要是針對光電太陽能元件的光學特性之基礎研究，其成果包括三個研究方向：（一）(一)利用周期性寬頻高效率光場增強陣列光子晶體，提出新式太陽能電池結構，並將光譜分離式共振腔結構應用於多接面太陽能電池上(high-efficiency resonant-cavity-like structures for multi-junction or multi-band solar cell application)。相對於隨機幾何繞射結構，周期性的結構可提供可重複且較穩定的效率轉換。在這一次的計畫之中，我們運用了表面電漿子陣列(surface plasmon array)，來提供光場增強的效應，透過在薄膜太陽能電池的上下兩端的表面電漿子陣列。我們形成了一個共振腔結構，進而達到相當良好的光場增強效應和效率提升。(二) 本計畫之第二個研究方向，為進行光學特性的基礎研究，以增進對太陽能電池中，光場增強效應(Light Trapping) 之深入了解。這一個研究之重點 在於計算太陽能電池之光學特徵模式(eigen mode)。在了解了特徵模式之後，在進一步研究導膜共振(guided mode resonance)之形成，和如何增強此一共振並達到寬頻增益。(三) 進行隨機幾何形狀應用於太陽能電池底部反射鏡(back reflector) 之研究，將利用基因演算法來進行幾何形狀之最佳化，決定最適合運用在太陽能電池的幾何形狀。在這一次的計畫中，最佳化之隨機幾何底部反射鏡的效率，相比於週期性陣列，可以達到~30%之提升。

本計畫的執行得到了下面的成果：(I)前瞻光學共振腔型態元件的提案，將提供未來高效率太陽能電池的設計藍圖 (II)證實/示範運用奈米光學模擬可以有效的提升太陽能電池的設計，並透過有效的光場增強效應，太陽能電池的吸收與轉換效率可以得到顯著的提升，(III)透過特徵模式的分析、透射/反射/吸收頻譜的計算、和繞射級數的計算，提升對於太陽能電池基礎物理的了解，尤其是光子在元件中折射/反射/繞射的現象(IV)隨機幾何底部反射鏡之設計，將可以進一步提升薄膜矽太陽能電池的效率。

Abstract

Keywords: solar cell, resonant cavity, randomized reflector, eigen mode

This research report is mainly for the fundamental research of photovoltaic device optics. The achievement can be separated into three parts (I) Cavity-resonant solar cells using subwavelength gratings, and application of cavity-resonant structure to multi-junction cells. The specific design in this study using plasmonic effect, which can enhance the spectral splitting through surface plasonic subwavelength grating and therefore increase the photocurrent of multi-junction cells. (II) The second effort in this proposal is the fundamental understanding of light trapping phenomenon in photovoltaic cells. Specifically, the eigen mode and photonic bandstructure is studied, and their effect on the absorption enhancement is assessed. It should be noted that only through properly designed quasi-guided mode excitation, the thin-film solar cells can achieve their ultimate efficiency for a given active layer thickness. Other photonic enhancement approaches such as slow light and resonance enhancement are also preliminarily studied in this project. The last research effort of this project is (III) Improved randomized grating structures for high efficiency solar cells, through genetic algorithm optimization, and based on the physics studied in goal (II). The conventional randomly textured silver-dielectric back reflectors are widely used in commercial solar cells. Nonetheless, well-designed random structures have not been carefully examined and not been made possible. In this project, a lithographically definable random reflector is proposed, and its efficiency is shown to be ~30% higher than its periodic counterpart.

The success of this project contribute in (I)New/Novel/Promising optical cavity structures proposal provides directions for future high efficiency solar cell design. (II) Demonstration of using nano photonic modeling approach to design solar cell optical structures. (III) Improving the fundamental understanding of electrodynamic phenomenon inside solar cells by eigen mode analysis, transmission/reflection/absorption calculation, and diffraction order analysis. (IV) Design of randomized structures benefiting future high efficiency thin-film solar cells.

一、 前言

隨著化石能源(fossil fuel)之漸漸枯竭和核能安全的問題，再生能源已成為近年來最重要之研究議題。在所有的再生能源之中，太陽能技術是最成熟，且最有希望在近期內去取代傳統的電力產生設備，然而，此一產業所面臨的最大問題，是 $/Watt 依然居高不下，尤其是相對於現有的發電技術，因此，為了要使太陽能技術能普及化，降低成本與提升效率是雙軌並行的兩個重要方向。

值得一提的是，現在產學所關注的第三代太陽能電池，也即多重接面太陽能電池(multi-junction solar cells)和雜質能帶太陽能電池(intermediate band solar cells)，需要大量的光學最佳化。以多接面太陽能電池來說，其越薄的材料主動層厚度越能降低本，此在薄膜吸收不足的情形之下，光學的設計更顯重要。儘管近幾年大量的研究被投入在太陽能電池的光學特性上，如何設計出有效的光場增強結構，如何產生寬頻大角度以及偏振不敏感(polarization insensitive)共振腔結構的方法，依然不清楚，對於該以甚麼參數來衡量一個太陽能電池的光學特性和設計之好壞，也尚未明朗。古時候以光軌跡長度(optical path length)來衡量太陽能電池設計的優劣，已經無法準確的描述以奈米薄膜為主的第二、三代太陽能電池，如果可以從基礎的物理層面著手，則很有希望去發現其中的關鍵。

二、 研究目的

Dielectric Mirror and Broad Angel Reflectors and Cavity-Resonant Solar Cells 介電質反射鏡與共振腔式太陽能電池

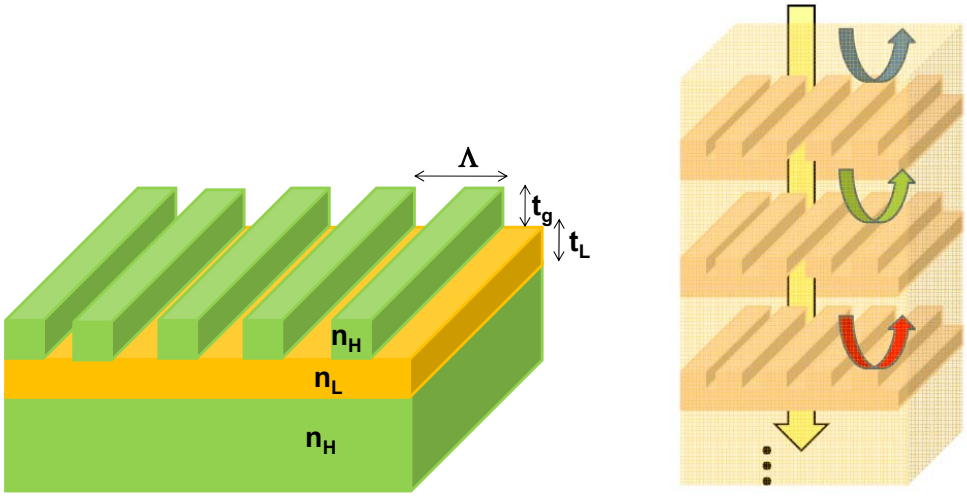

Fig. 1 (Left) Illustration of broad band dielectric mirror and (Right) Cascaded resonant cavity type solar cell

底部反射鏡通常可以增加太陽能電池的吸收，尤其是在薄膜太陽能電池的應用上，因為材料的厚度不夠，在長波長(紅光)的波段，必須透過底部反射鏡來增加吸收效率[1-15]。光子在進入元件之後，如果其波長落在材料的吸收頻譜當中，就會漸漸的被材料吸收，當材料的吸收係數不夠(e.g.紅光)時，或是材料的厚度不足時，(如薄膜太陽能電池)，則大部分的光子會在經過整個元件的長度之後，而到達元件的底部，此時，若是沒有底部反射鏡存在，則反射就只能靠半導體和空氣間的折射率差異，一大部分的光子將進入環境(ambient)之中，而無法貢獻光電流。設計得當的底部反射鏡，可以達到 85%以上的反射，因此是太陽能電池技術當中，不可或缺之元素。

傳統的金屬反射鏡[2, 4-6, 14]，如銀、鋁、或是不鏽鋼，都可被應用在太陽能電池中。銀可以提供高的反射係數，鋁是傳統矽製程作為導線的材料，而不鏽鋼則可以作為堅固的基板(substrate)。金屬底部反射鏡面臨的問題，包括在短波長時的低反射和高損耗(e.g. 表面電漿子吸收)，因此若要將金屬反射鏡應用在整個太陽能頻譜，是無法達到寬頻高反射的效果。當然不可否認的，金屬反射鏡依然是目前工業化太陽能電池的主流，它有製程和設計的簡便性，尤其在設計上，金屬的沉積厚度若些許變異對於底部反射鏡的反射能力都沒有顯著的影響，這和介電質反射鏡(dielectric mirror)必須精密控制厚度是很不一樣的。

介電質寬頻反射鏡可以提供更高的反射[16]，主要是由於它的所依賴的是折射/反射/繞射/干涉的現象，來產生高反射結果，因而沒有如金屬會因吸收係數隨波長變化和表面電漿子吸收效應，造成在某些波段中之低反射現象。此外，由於沒有金屬層，製程的溫度可以大幅提高，這是附帶的好處。不過在設計上的複雜度，將比較高。尤其是如何選取對的幾何參數，將會是一個挑戰。而介電質寬頻反射鏡相較於金屬反射鏡，有另一缺點，即介電質寬頻反射鏡通常是有方向性的，也就是說，當入射光的波向量(wave vector)角度有所變化時，或是入射光偏振方向(polarization angle)有變化時[17]，電質反射鏡的光學特性，將會不同，因此，如何透過電磁理論計算，來得到好的低方向依賴性(low angle dependence)的光學結構，將是未來介電質寬頻反射鏡，是否能成功應用薄膜太陽能電池上的重要關鍵。

其中一種介電質寬頻反射鏡，是所謂的分散式布拉格反射鏡(Distributed Brag Reflector)，其結構為不斷重複之交替沉積的兩種材料(ABABAB)，其原理為，若是電磁波經過連續的反射，所產生的反射波之相位皆相同時，就產生了所謂的建設性干涉，因此，整體上的反射能力，將會是很大的(>99%)。分散式布拉格反射鏡的理論基礎是相對簡單，因此很快的被學術人士接受，且應用在多種光電元件中，最有名的是垂直共振腔表面發射雷射(VCSEL)[7]，這一光電元件的成功運作，也間接證實了分散式布拉格反射鏡的可行性和其理論基礎。必須要點出的是，分散式布拉格反射鏡的反射能力，和材料的折射係數差異(refractive index contrast)，有很大關係，一搬來說，越大的折射率差，可以提供越高的反射能力，且布拉格反射鏡所需要的重複組數(number of pairs)也越少，另外，由於分散式布拉格反射鏡是一維的結構，它對於入射波的方向和偏振有較輕的依賴，這是好的，不過由於為了達到高反射能力，往往大數量的重複組數(number of pairs)必需被沉積，這會增加元件的厚度，和製程的複雜性。

另外一種形式的介電質寬頻反射鏡，是所謂的高折射係數反差光柵結構(High Refractive Index Contrast Gratings)，最早在 2004 年由 Connie J. Chang-Hasnain 提出[16]。由兩種不同的材料來組成的光柵，由於折射係數的差異，造成很強的反射能力，而其反射能力的好壞，與兩種材料的折射係數差也是有很大的關係，越大的差異可以造成越好的光學反應。此外，光柵的幾何尺寸，也是造成寬頻高反射能力之關鍵，因此，對於幾何參數之設計，也是高折射係數反差光柵結構成功的關鍵。造成高反射能力的基礎物理原因，現在還不是很清楚，一般來說，導模共振(guided mode resonance)被認為是造成高反射現象的原因。從模擬上可以看到的高反射現象，已經從實驗上得到一些間接的映證[18-21]。傳統的 VCSEL 上下兩面必須以前面提到的分散式布拉格反射鏡，來作為雷射腔的反射鏡，由於 VCSEL 的共振腔很短(因其垂直的特質)，所以其兩面的反射鏡必須具有很高的反射係數，才能達到增益(gain)的結果，若是用布拉格反射鏡來做，則需要用約 40 對的交替(pairs)才能達到高於 99%的反射，因此，造成元件的厚度變大且製程步驟變多，若是改成光柵形式的反射鏡，則可以大大減低製程的複雜度和元件的厚度。實驗上以光柵取代部分的分散式布拉格反射鏡，在 VCSEL 上已可以看到會運作的雷射現象。

光柵形式的反射鏡可分成一維和二維光柵，一維光柵的光學反應具有偏振的依賴性，可以用在如量子井雷射或偏振器(polarizer)上，而二維光柵可以做到偏振不敏感，因此可以用在紅外線感測器和太

陽能電池上，值得一提的是，由於麥斯威爾方程式(Maxwell's Equation)具可擴縮性(scalability)，即：

$$\kappa^2\left[\frac{\partial^2 E(x,y,z)}{\partial x^2}+\frac{\partial^2 E(x,y,z)}{\partial y^2}+\frac{\partial^2 E(x,y,z)}{\partial z^2}+\omega^2\mu\epsilon(x,y,z)E(x,y,z)\right]=\kappa^2\times 0=0 \quad (1)$$

經過數學推導可得

$$\begin{aligned}&\frac{\partial^2 E(x,y,z)}{\partial(x/\kappa)^2}+\frac{\partial^2 E(x,y,z)}{\partial(y/\kappa)^2}+\frac{\partial^2 E(x,y,z)}{\partial(z/\kappa)^2}+(\kappa\omega)^2\mu\epsilon(x,y,z)E(x,y,z)\\ &=\frac{\partial^2 E(\kappa x',\kappa y',\kappa z')}{\partial(x')^2}+\frac{\partial^2 E(\kappa x',\kappa y',\kappa z')}{\partial(y')^2}+\frac{\partial^2 E(\kappa x',\kappa y',\kappa z')}{\partial(z')^2}\\ &\qquad+(\kappa\omega)^2\mu\epsilon(\kappa x',\kappa y',\kappa z')E(\kappa x',\kappa y',\kappa z')\\ &=0\end{aligned} \quad (2)$$

因此，等比例的縮放可以將光柵的光學反應，在頻譜的橫軸上平移，所以，同樣的一個設計，只要經過尺寸縮放，便可以應用在不同的波段。

Fundamental Understanding on Solar Cell Light trapping

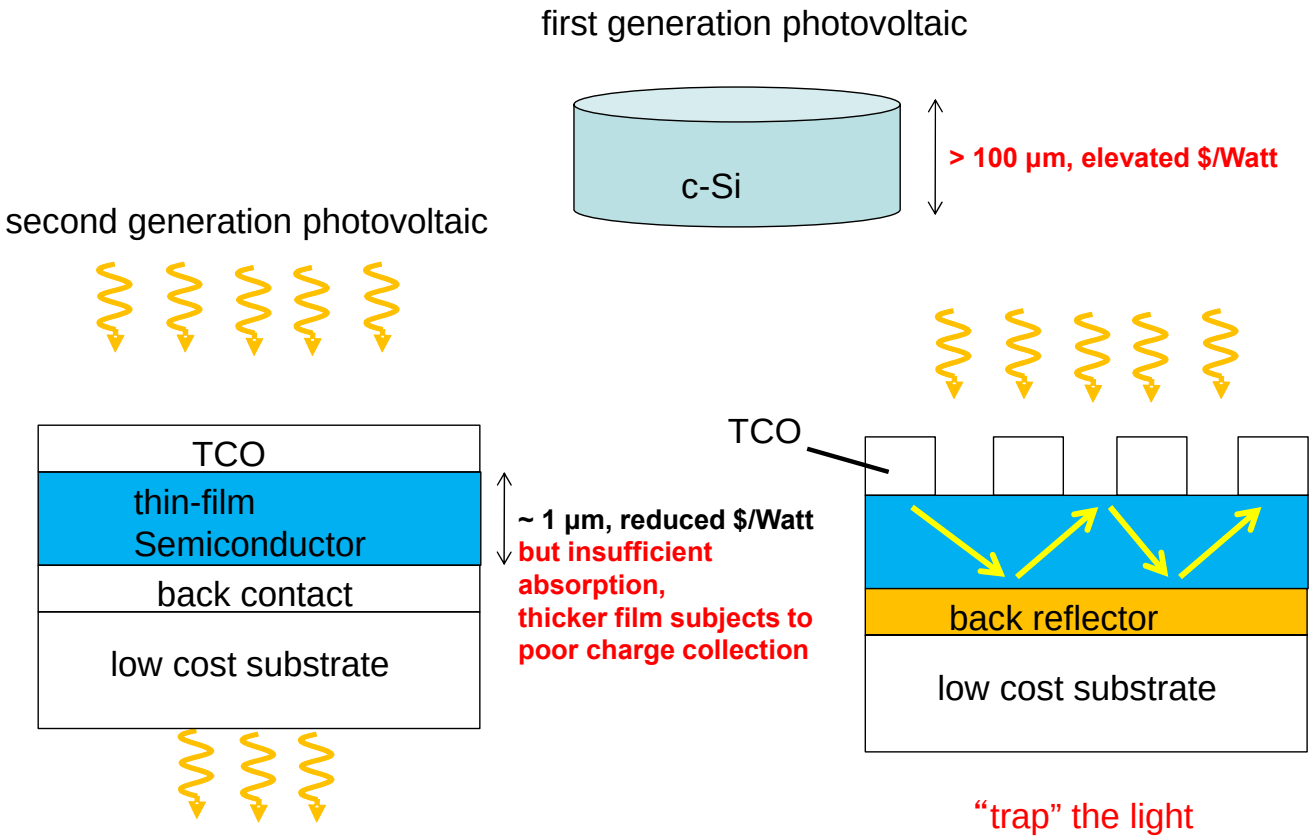

Fig. 2 Illustration of importance of light trapping in thin-film photovoltaics

早期的太陽能電池，皆以矽晶圓製造為主，其厚度約在 200 μm 至 300μm 之間，這樣的太陽能電池，有許多缺點，包括消耗掉大量的矽原料，因此價格偏高，重量偏重，且其轉換效率在非高密度太陽能電池情形下，(即 under one sun condition)，受限在 20%左右[22]。新一代的太陽能電池，將以薄膜為主，包括矽(單晶、多晶、非結晶)、矽鍺化合物、銻化鎘(CdTe)、銅銦鎵硒(CIGS)、和各種有機化合物等材料，因為是薄膜，對於光子的吸收並不完全，因此必需透過適當的光場增強，才能充分的利用太陽光的能量。

傳統上來說，太陽能電池的光學特性，可以用光跡追溯技巧(ray tracing techniques)[8]，和光學軌跡長度參數(optical path length)來衡量。光跡追溯技巧的執行，是先將整個元件分割成細小網格，光源由上往下照射，藉由簡單的折射反射定律，光在計算區域的強度分佈便可知道，這一種方法的缺點是將光看待成純量，其電磁波的特性，也就是干涉繞射等波動現象，並不能適當地被描述。因此，在評估傳統的矽晶圓太陽能電池上，光跡追溯技巧(ray tracing techniques)，是合理有效之方法，然而對於薄膜太陽能電池，由於光在薄膜的強烈繞射效應，更準確的電磁理論與數值方法，是達到更高轉換效率的必要元素[3, 5, 6]，此外，由於薄膜太陽能電池對光子的吸收較弱(薄膜的特性)，因此有效的光學設計，將是此新一代太陽能元件，可否能成功推行至商業化之關鍵。

值得一提的是，現在產學所關注的第三代太陽能電池，也即多重接面太陽能電池(multi-junction solar cells)[23]，和雜質能帶太陽能電池(intermediate band solar cells)[22]，也需要大量的光學最佳化。以雜質能帶太陽能電池來說，其材料不論是量子點或是高度不吻合合金(Highly Mismatched Alloy)，其電子擴散長度(diffusion length)皆偏短，因此元件之主動區域不能太厚，在薄膜吸收不足的情形之下，光學的設計更顯重要。儘管近幾年大量的研究被投入在太陽能電池的光學特性上[1-6, 24-33]，如何設計出有效的光場增強結構，如何產生寬頻大角度以及偏振不敏感(polarization insensitive) 結構的方法，依然不清楚，對於該以甚麼參數來衡量一個太陽能電池的光學特性和設計之好壞，也尚未明朗。古時候以光軌跡長度(optical path length)來衡量太陽能電池設計的優劣，已經無法準確的描述以奈米薄膜為主的第二、三代太陽能電池，如果可以從基礎的物理層面著手，則很有希望去發現並釐清其中的關鍵。

截至目前為止，大部分的太陽能電池光學特性的研究，是比較分散的概念，一般認為對於效率提升有幫助的現象包括了大角度的折射去增加紅外線的吸收，表面的抗反射薄膜去增加藍光的穿透，隨機幾何的底部反射鏡去提供寬頻的散射，以及在金屬和半導體之間加入折射係數約為 2 的介電值材料，去增加金屬底部反射鏡的反射效率，然而，這一些分散的概念，還必需要透過嚴謹的電磁理論和模擬，才能夠真正的找出可以用來衡量太陽能電池光學效率的參數或數個參數(figure of merit)，和具整體性規劃的設計規範。

Optimized diffractive element: Random gratings

隨機幾何形狀的光學結構，在實驗上、工業應用上早已行之多年[1, 3, 5]，一般來說，在沉積太陽能電池薄膜的製程當中，就可以藉由溫度和壓力的變化，來產成顆粒大小形狀隨機分佈的表面，這個

表面就被用來當做散射太陽能光子的工具。

光子經隨機幾何形狀的結構反射，可以產生藍伯(Lambertian)分佈[7]，這對於大角度的去散射光子是很有幫助的，因此，有許多太陽能電池，使用隨機幾何的結構，作為有效的底部反射鏡，然而，這一種隨機式的反射結構，可能會造成所生產生的太陽能電池之轉換效率，會有一定程度的變異，也就是說，無法有效的控制樣本的品質，這對大量生產和商業化來說，是不好的因素。此外，隨機幾何的形狀，並無經過最佳化，是否為最佳的解，並無法得到證實。

如果透過適當的設計，可以使太陽能電池的效率提升數個百分點，因而降低$/Watt，則對於太陽能電池大眾化將會有顯著的幫助。尤其重要的是，相對於其他太陽能電池效率提升的方法，包括雜質能帶(超高效率太陽能電池 Ultra High Efficiency Photovoltaics)，有機薄膜(低價大面積)，量子結構(改變材料電性)等，光學方法和光場增強的概念，是可以被應用在任何一種太陽能電池技術(材料架構)上的，其並無技術上的困難，未來也有機會做到不增加生產成本，而所缺少的只是理論的計算、適當的設計、和嶄新的觀念。

三、 文獻探討

Cavity resonant type solar cell and eigen mode excitation

The use of multi-junction cells, which are occasionally referred to as tandem cells, is a practical method to exceed the Schokley and Quessier limit of photovoltaic devices. Recently, surface plasmon (SP) photovoltaics has drawn considerable attention because it can provide a new route to improve thin-film solar cell light-trapping below the diffraction limit [24, 27-31, 34-50]. The surface plasmon phenomena that have been related to photovoltaics include localized surface plasmon (LSP) [28, 29, 34, 38, 51], surface plasmon polariton (SPP) [34, 36, 37, 45, 51], and far-field enhancement. Previous studies included a single metallic nano-particle array on the top of a semiconductor layer [29, 34, 45, 52] to enhance photon forward scattering, and plasmonic back reflectors showing SPP propagation along the metal/semiconductor interface [34, 36, 37, 45, 51]. Although a single metallic grating on the top or on the bottom of the semiconductor thin-film effectively improved solar cell efficiency, cavity design is necessary to improve the efficiency even further. Here, the SP cavity design was applied to the multi-junction cells. For multi-junction cells, current matching is the most important consideration to maximize the efficiency; therefore, the subcells should have matched integrated absorbances. To optimize the geometrical parameters, a genetic algorithm (GA) was employed in this study. GA is a global search method that mimics natural evolution. It can identify a global maximum for ill-behaved objective functions, such as the optical cavity design, which is impossible to achieve using conventional optimization methods. The micromorphic silicon multi-junction cell was used as an example to demonstrate the effectiveness of GA-optimized SP cavity for spectral flux management in the multi-junction cells. Micromorphic multi-junction cells normally require a thick microcrystalline silicon (μc-Si) bottom cell due to the low absorption coefficient of μc-Si. Therefore, a surface plasmon micro-cavity can be employed to improve the absorbance of the μc-Si bottom cell and the current matching of the entire multi-junction cell.

Fundamental understanding of solar cell light trapping

Periodic grating can enhance solar cell absorbance by providing quasi-guided mode excitations[26, 30, 34, 35, 38, 40, 43, 45, 48, 49, 51, 53-55]. Nonetheless, quasi-guided modes cannot exist over the entire solar spectrum due to its discrete nature. The question arises: How to utilize the limited-number, non-continuous qausi-guided modes to maximize the short circuit current. Previously, it has been assumed that the broad band absorbance enhancement is proportional to the number of guided mode peaks[30, 54]. The work from the same authors later propose a distinction to the mode quality in terms of its overlap-integral[56]. More recent experimental work studies the dispersion and the absorption enhancement, and motivates the concept that mode confinement, i.e. Q-factor, also plays an important role in determining the broad band absorbance[53]. It is also interesting to know whether it is more efficient to use narrow band high-Q peaks or to use fewer broad band low-Q peaks, to cover a specific spectral range. In this work, it is shown that while the number of guided mode peaks has pronounced effect on the short circuit current, other factors such as the mode quality and the

mode excitation wavelength and strength also affect the short circuit current. This leads to the observation that the solar cell geometry giving the most guided modes does not coincide with the geometry giving the highest short circuit current. In this work, the solar cell geometry is optimized using global optimization algorithm[57] to maximize the short circuit current at light trapping wavelength($J_{SC,LT}$), and the resulting spectral response is analyzed and compared. The investigation is conducted for the absorption enhancement by the non-plasmonic and plasmonic back reflectors, respectively, since the non-plasmonic and plasmonic back reflectors are expected to exhibit different natures. The optimization is repeated for several runs to confirm the result, and very similar conclusion is arrived. For non-plasmonic solar cell back reflectors, it is found that the modes are mostly of diffractive nature. The excited modes exhibit high-Q resonance and the air-dielectric-semiconductor-metal essentially acts as a conventional index-guided waveguiding structure. On the other hand, surface plasmon(SP) has long been known for its broad band emission[38, 40, 43, 45, 48, 49, 55] capability. Aaccording to the study here, the quasi-guided modes associated with plasmonic back reflectors without a dielectric spacer exhibit low-Q broad band resonances and the absorbance enhancement is mostly through the broad band coverage of solar spectrum. This is pronouncedly different from the high-Q diffractive modes for the non-plasmonic back reflectors.

Optimized diffractive element: Random gratings

Random reflectors are always of particular interest for solar cell. The optimized random geometry can potentially exceed the so-called Lambertian limit[1, 5, 7, 9, 11, 12, 14, 58-62]. There are several issues associated with optimized random geometry. (1) The optimized random profiles are usually very difficult to fabricate. (2) The randomized nature results in that the geometrical construction of conformal layers is quite difficult. The suitable geometrical definition of such a full 3D structure is inevitable, if the solar cell geometry is going to be optimized by a particular optimization algorithm. The geometry has to be adjusted automatically during optimization, rather than adjusted manually at each run. (3) The full three-dimensional(3D) solar cell structure with a random back reflector, a dielectric spacer, a conformal semiconductor layer, and a front-side anti-reflection coating has not been optimized to date due to its large computational demand.

Here a global optimization algorithm together with a geometrical parameterization procedure is proposed for designing optimal random gratings for future thin-film photovoltaics. There are several potential methods for global optimization, and genetic algorithm is selected here due to its versatility and the fact that it does not require initial guesses. The proposed method can be applied to solar cells using any materials although a silicon thin-film is used in this study. In literature, optimization of one dimensional(1D) randomized profile for solar cells has been reported [26, 33] using 2D simulation. Nonetheless, in these works the optimized 1D profile is difficult to fabricate while two dimensional(2D) grating geometry in three dimensional(3D) simulation is much preferred in real devices due to its higher absorbance enhancement. The initial result of this work can be found in [63].

四、 研究方法

Cavity resonant type solar cell and eigen mode excitation

Using multi- junction cell is a practical way to exceed Schokley and Quessier limit of photovoltaic devices. Recently surface plasmon(SP) photovoltaics draws consideration attention, which provides a new route to further improve thin-film solar cells light-trapping below diffraction limit [24, 27-31, 34-49]. This includes localized surface plamon (LSP) [28, 29, 34, 38, 51], surface plasmon polariton (SPP) [34, 36, 37, 45, 51], and photon re-emitted back into the semiconductor thin-film by surface plasmon, leading to far-field enhancement. Previous work includes a single metallic nano-particle on the top of semiconductor layer[29, 34, 45, 52], which shows enhanced photon forward scattering into silicon, and plasmonic back reflectors which in general shows SPP propagating along the metal/semiconductor interface[34, 36, 37, 45, 51]. Although a single metallic grating on top or bottom of semiconductor thin-film has been shown to be effective for improving solar cell efficiency, cavity-design is expected to improve the efficiency even further. With photonic cavity, photons can be trapped inside absorbing thin-film. In conventional thin-film photovoltaics, the trapping is due to total internal reflection (TIR) where photons outside escape cone can be totally reflected back into semiconductor thin-film. In SP cavity, absorption and remitting of photons by SP, together with LSP and SPP, can further improve the light trapping capability of photonic device, provided proper optimization can be achieved. For optimization of geometrical parameters, genetic algorithm (GA) can be used. GA is a global search method and mimics natural evolution. It can find global maximum for ill-behaved objective functions such as the case of optical cavity design. This is impossible to achieve using conventional optimization methods. The micromorphic silicon tandem cell can be used as example to demonstrate the effectiveness of GA optimized SP cavity for solar spectral flux management. Micromorphic cell normally requires thick mircrocrystalline silicon (μc-Si) bottom cell in order to have higher absorbance for long wavelength photons due to lower absorption coefficient of μc-Si. Surface plasmon microcavity canthus be employed to improve μc-Si bottom cell absorbance and current matching. Fig. 3 illustrates the two types of cavity plasmonic design including intermediate reflector and bottom grating(IRBG) cavity and top and bottom grating(TBG) cavity.

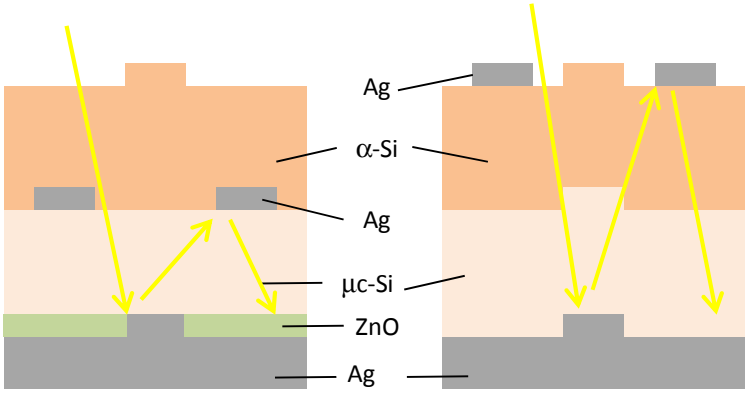

Fig. 3 Example of (Left) intermediate reflector and bottom grating (IRBG) cavity, (Right) top and bottom grating (TBG) cavity.

Fundamental understanding of solar cell light trapping

In this work, the discretization of Maxwell's equation is carried out by two-dimensional finite element method, using COMSOL Multiphysics software package [64]. Periodic boundary conditions are set at the left and right boundaries, while perfectly matched layer absorbing boundary conditions are used at the top and bottom boundaries of the computational domain. The absorbance in silicon is then calculated by integrating the divergence of the time-averaged Poynting vector, which is then normalized by the incident power. Only absorbance in silicon generates electron-hole while absorbance in metal leads to surface plasmon absorption loss. The details of the calculation can be found in reference[6-8, 26, 64]. The absorbance is calculated by integrating the power dissipation in silicon:

$$\mathrm{A}(\lambda) = \frac{\frac{1}{2}\int_V \omega\varepsilon_0\varepsilon''(\lambda)\left|\vec{E}(\vec{r})\right|^2 dv}{\frac{1}{2}\int_S \mathrm{Re}\left\{\vec{E}(\vec{r})\times\vec{H}^*(\vec{r})\right\}\cdot d\vec{s}} \tag{3}$$

where ω is the angular frequency, λ is the free space wavelength, ε_0 is the permittivity in vacuum, and ε'' is the imaginary part of complex semiconductor dielectric constant. The short circuit current at light trapping wavelength, $J_{\mathrm{SC,LT}}$(600nm-1000nm) is calculated by averaging A(λ) weighted by AM 1.5 solar spectrum:

$$J_{\mathrm{SC,LT}} = q\int \frac{\lambda}{hc}\Omega(\lambda)\mathrm{A}(\lambda)d\lambda \tag{4}$$

where $\Omega(\lambda)$ is AM 1.5 solar spectrum in unit of J $s^{-1}cm^{-2}$ nm^{-1}, h is the Plank constant, λ is the free space wavelength, q is the elementary charge, and c is the speed of light in vacuum. The genetic algorithm is chosen as the global optimization techniques for locating the optimized geometry for the periodic grating on the solar cell back reflector. It is chosen due to the fact that the genetic algorithm has been proved to be very effective in different engineering fields[65-68]. During the optimization procedure, the objective function is defined as the short circuit current at light trapping wavelength($J_{\mathrm{SC,LT}}$), which is to be maximized by adjusting grating geometry. The objective value will keep increasing and then saturate, as the optimization goes on. When the optimization runs for long enough time, the objective value will gradually converge to the global maximum of the objective function. In order to reveal the relationship between the number of supported quasi-guided modes and $J_{\mathrm{SC,LT}}$, the number of qausi-guided modes for each individual(sample) is monitored during the optimization procedure. To strengthen the conclusion, several optimization runs are conducted and highly similar result and observation are arrived, and the result is included in the following sections.

The first structure under study is a silver back reflector directly in contact with silicon. TE polarization and TM polarization in two-dimensional(2D) simulation domain are used to study the non-plasmonic back reflector and plasmonic back reflector respectively. Using TM polarization in 2D simulation domain to study the plasmonic structure has been employed [29, 34], and the structures with direct contact of metal-semiconductor are commonly referred to as plasmonic back reflectors or plasmonic structures[34, 51]. Afterward, the effect of dielectric spacer on plasmonic structures is studied to reveal the effect of dielectric shielding on the surface plasmonic absorption. For dielectric spaced structure, only TM polarization is studied

since TE polarized light does not excite surface plasmon[29, 34] and its metallic loss is much alleviated compared to TM polarization. It should be pointed out that plasmonic structures(TM) can initiate both plasmonic and non-plasmonic modes. On the other hand, non-plasmonic structures(TE) do not possess surface plasmon excitation capability.

The study is arranged as follow: Firstly the relationship between quasi-guided modes and absorption enhancement is conducted, for non-plasmonic(TE) and plasmonic(TM) back reflectors, respectively. Afterward, the usage of dielectric spacers on plasmonic structures and its effect on the optimal quasi-guided mode excitations are assessed. For the generalization to solar cells in three-dimensional(3D) domain, the non-plasmonic back reflector is more related to the solar cells with dielectric mirrors where all of the excited modes are of purely diffractive nature. For the plasmonic back reflector, it is more related to thin-film solar cells with 2D-textrued or 2D-grated metallic back reflectors. For 2D texturing/grating in 3D domain, surface plasmon absorption will exist for both polarizations. As a result, the SP absorption has to be mitigated by a dielectric spacer for both polarizations, which will be revealed later.

The film thickness is 0.3μm and poly-crystalline silicon (poly-Si) is used as an example to study different solar cell structures. For experimental poly-Si thin-film solar cell, the typical thickness is 1~2 μm. Here the thickness is kept thinner than full absorption to better reflect the light trapping effect. This is similar to Yu et al [54] where 3μm crystalline silicon is used for weak absorption while full absorption thickness of c-Si solar cells is around 200 μm. It should be emphasized that the conclusions drawn here do not only apply to poly-crystalline silicon, they also apply to other inorganic semiconductors as well. This is due to the similar mode coupling, light scattering, and waveguiding behaviors in inorganic solar cells. Crystalline silicon parameters have also been tested and the conclusion is the same except slightly lower short circuit current values. For organic solar cells, the near field enhancement is more dominant and the conclusions here may not apply. The wavelength range chosen is from 600nm to 1000nm which corresponds to the long-wavelength light trapping regime for silicon solar cells where the quasi-guided mode excitation is critical. The material refractive index and extinction coefficient is from Rsoft material database[69] and literature[9, 60, 70-73]. The CPU runtime for a single optimization run is around 72 hours using Intel quad-core Xeon 3.1GHz processor. It is worth mention that one-dimensional(1D) grating or texture is in 2D simulation domain, and 2D grating or texture is in 3D simulation domain. In the paragraph below, when 1D or 2D grating is mentioned, the specification of the simulation domain may be omitted but its meaning should be clear from the explanation above.

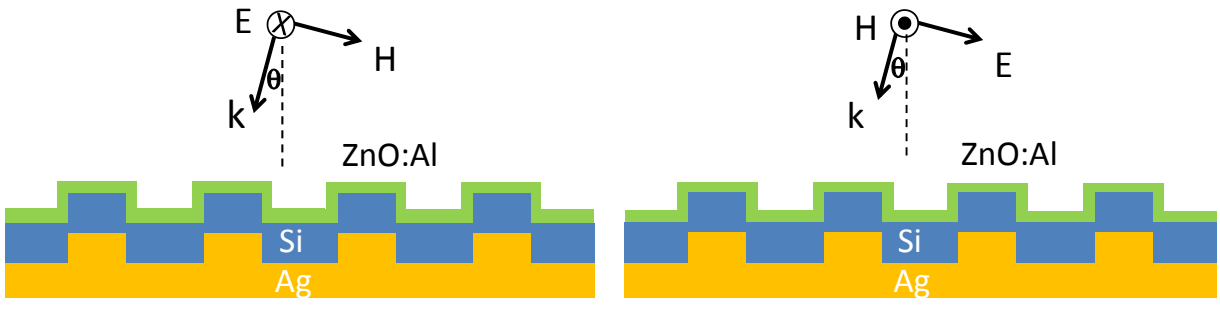

Fig. 4 The set-up for investigating non-plasmonic back reflectors (TE) and plasmonic back reflectors (TM) in two-dimensional space.

Optimized diffractive element: Random gratings

The evolutionary structure consists of ZnO/Si/ZnO/Ag, and the thickness of silicon is 700 nm, the thickness of layer 2 is 100nm, and groove height for the grating is 250 nm. The binary grating can be fabricated using usual lithography techniques in one etch step. Each binary bit is 250 nm in both width and length. The structure is defined using 7 layers. Layer 1 is a uniform Ag layer. Layer 2 is a uniform ZnO layer. Layer 3 is a ZnO/Si layer, which is defined according to the binary mask pattern as a function of 0 and 1, as shown in Fig. 5.

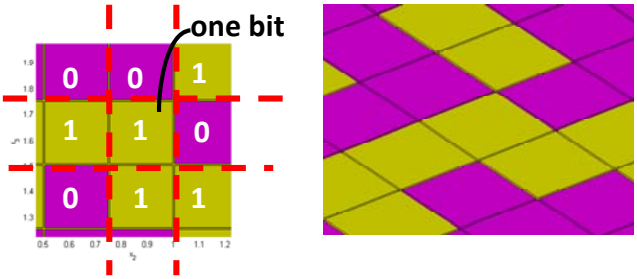

Fig. 5. (left) Illustration of the way to define layer 3 ZnO/Si and (right) 3D view.

The algorithm can be defined as below for layer 3:

$$\begin{aligned} &\textit{if} \quad \textbf{the binary mask is 1} \\ &\qquad n_r = n_{ZnO} \\ &\textit{else if} \quad \textbf{the binary mask is 0} \\ &\qquad n_r = n_{Si} \end{aligned} \tag{5}$$

1 represents the mesa and 0 represents the etched area. Therefore in (3), 1 represents ZnO while 0 represents silicon since the etched region will be conformally filled with silicon. Afterward, layer 4 is a uniform layer of silicon, whose thickness will be the total thickness minus the groove depth of the grating. Layer 5 is silicon/ZnO, and the initial binary mask can used to define the fifth layer. Layer 5 is part of the ZnO top contact conformal coverage.

Layer 6, which is the sidewall of the top silicon grating structure, is more complicated to define. The thickness of the sidewall is 50nm, which is assumed to be half of the film thickness of the topmost ZnO coverage. As illustrated in Fig. 6, the side wall definition can be done by dividing one bit of binary mask pattern into 9 sub-regions. Whether each sub-region should be air, silicon or ZnO is determined by whether its adjacent region is silicon or air and whether the underlying binary mask bit is 0 or 1. In addition, for each sub-region, the situation can be slightly different as stated below.

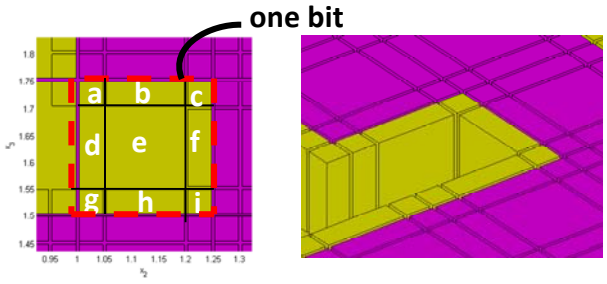

Fig. 6. (left) Illustration of the way to define layer 6 sidewall and (right) 3D view.

For the case of sub-region a, b, c, d, f, g, h, or i, if the underlying binary mask bit is 1, a ZnO grating bump is already defined in the layer 3 at this specific mask bit location. Thus in order to achieve conformal coverage, silicon refractive index is used. In the case that the underlying binary mask bit is 0, which means at this specific mask bit location a ZnO grating dip is already defined in layer 3, the sub-region in the layer 6 should be air or ZnO, depending on whether any of the adjacent regions is silicon or not. If any of the adjacent regions is silicon then ZnO refractive index is used since the sub-region in this case should be the ZnO sidewall of the adjacent silicon material.

$$\begin{aligned} &\textit{if} \quad \textbf{the binary mask is 1} \\ &\qquad n_r = n_{Si} \\ &\textit{else} \\ &\qquad \textit{if} \quad \textbf{one of the adjacent region is silicon} \\ &\qquad\qquad n_r = n_{ZnO} \\ &\qquad \textit{else} \\ &\qquad\qquad n_r = n_{air} \end{aligned} \tag{6}$$

For sub-region e, the situation is simpler. If the underlying binary mask bit is 1, which means a ZnO grating bump is already defined in this specific mask bit location in layer 3, silicon refractive index is used to construct the conformal coverage of silicon thin-film. Otherwise if the mask bit is 0, air refractive index is used.

$$\begin{aligned} &\textit{if} \quad \textbf{the binary mask is 1} \\ &\qquad n_r = n_{Si} \\ &\textit{else} \\ &\qquad n_r = n_{air} \end{aligned} \tag{7}$$

Layer 7 is the topmost ZnO front contact coverage, which constitutes part of the top ZnO conformal coverage. The thickness of the layer 7 ZnO coverage is 100nm. The definition can be extended from layer 6 using the same sub-region method as depicted in (4) and (5). Material optical constants can be found in literature [9, 70, 71, 73-77].

五、 結果與討論

Cavity-resonant type solar cell and eigen mode excitation

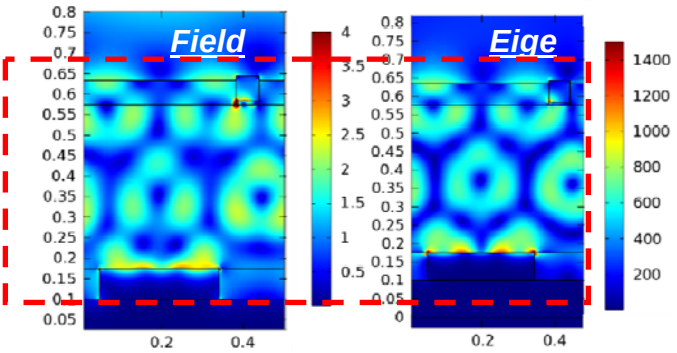

Fig. 7 Example of (Left) Field profile for scattering problem and corresponding (Right)Eigen mode.

Fig. 7 shows an example cavity resonant type solar cell where the similarity between field profile of scattering problem and eigen mode problem exists. SP single grating has been shown to be effective when placed on top of semiconductor thin film or above metal back reflectors. Nonetheless, the combined structure with both top and bottom grating that enables optimal cavity design has not been investigated. Here two type of cavity, i.e., plasmonic intermediate reflector & bottom grating(IRBG) and plasmonic top & bottom grating (TBG) are proposed and their capability to improve absorbance is studied. For SP intermediate reflector & bottom grating, structure consists of Ag back reflector/Ag&ZnO bottom grating/μc-silicon thin-film/ Ag intermediate reflectors/ α-Si thin-film, for SP top & bottom grating, structure consists of Ag back reflector/Ag bottom grating/μc-silicon thin-film/ α-Si thin-film/ Ag top grating. The optimization is done by adjusting each geometrical parameter until highest absorbance is found. Poynting vector and absorption power density which characterizes incident power per unit area and absorbed power per unit volume respectively can be written as

$$\begin{aligned} P_{\text{poynintg}} &= \vec{E}(\vec{r}) \times \vec{H}(\vec{r}) \\ P_{\text{absorption}} &= \vec{E}(\vec{r}) \cdot \vec{J}(\vec{r}) \end{aligned} \tag{8}$$

The electromagnetic field is essentially a time-varying field and time-averaged quantity is of interest as far as calculation of absorbance is concerned. The Poynting theorem, under harmonic steady state, states that time-averaged inflow power equals the time-averaged absorbed power.

$$\begin{aligned} &\int_V P_{\text{absorption, avg}} dv + \oint_S \vec{P}_{\text{poynintg, avg}} \cdot d\vec{S} \\ &= \frac{1}{2}\int_V \text{Re}\left\{\vec{E}(\vec{r}) \cdot \sigma(\lambda)\vec{E}^*(\vec{r})\right\} dv + \frac{1}{2}\oint_S \text{Re}\left\{\vec{E}(\vec{r}) \times \vec{H}^*(\vec{r})\right\} \cdot d\vec{S} \\ &= 0 \end{aligned} \tag{9}$$

where σ is conductivity of materials. The absorbance is the fraction of power absorbed divided by incident

power which is solar spectrum.

$$A(\lambda)=\frac{\frac{1}{2}\int \mathrm{Re}\left\{\sigma(\lambda)\vec{E}(\vec{r})\cdot\vec{E}^{*}(\vec{r})\right\}d\vec{r}}{\frac{1}{2}\int \mathrm{Re}\left\{\vec{E}(\vec{r})\times\vec{H}^{*}(\vec{r})\right\}\cdot d\vec{S}} \tag{10}$$

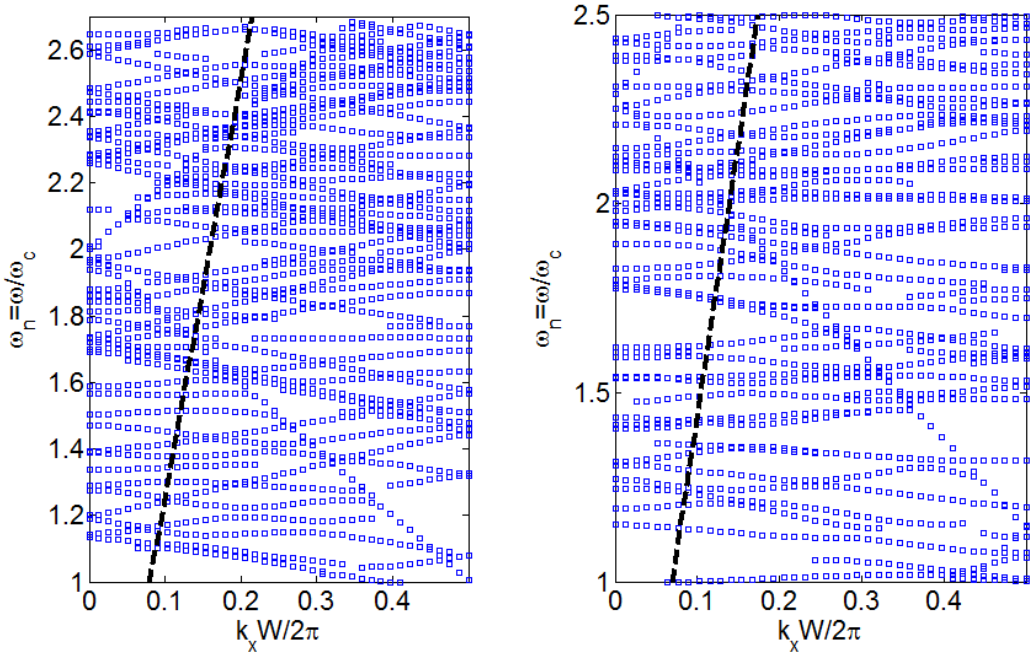

Fig. 8 Example of Line cone(black line) and photonic bandstructure for (Left)IRBG and (Right)TBG cavity-resonant type solar cell

Fig. 8 shows the photonic band structure for two types of cavity resonant solar cell. The frequency is normalized according to

$$\omega_{\mathrm{n}}=\omega/\omega_{\mathrm{c}}=\hbar\omega/E_{\mathrm{G,\,\alpha\text{-}Si}} \tag{11}$$

where ω_{c} is the cutoff wavelength of tandem cell which is taken to be 1000nm here. Bloch theorem states that photons in periodic structure can propagate without scattering and thus the photon lifetime can be extended if geometry is optimized. The photonic bandstructure can be utilized to observe quasi-guided mode excitation [28, 42, 46]. For any incident angle, a line can be drawn to characterize the relationship between ω and k_{x}:

$$k_x=k_0\sin\theta=\omega\sqrt{\mu\epsilon}\sin\theta \tag{12}$$

where k_{x} is in-plane wavevector, k_0 is wavevector in vacuum, ω is angular frequency, μ and ε is permeability and permittivity, and θ is incident angle. The corresponding incident field is

$$\bar{H}_{inc}(x,y)=H_{\mathrm{Z},0}\exp(jk_0x\sin\theta\text{-}jk_0y\cos\theta) \tag{13}$$

The intersection between the line (Eq.(9)) and the photonic bandstructure is where quasi-guided mode excitation is likely to exist. The line cone corresponds to incident angle of 90° and the y-axis corresponds to normal incidence. The Bloch periodic wave function in the SP cavity is

$$\vec{H}(\vec{r}) = \vec{H}_{\mathrm{P}}(\vec{r}) \exp(j\vec{k}_{\|} \cdot \vec{r}) \tag{14}$$

where $k_{\|}$ is in-plane wavevector and H_{P} is periodic modulation. The eigen mode excitation condition can be written as:

$$\vec{k}_{\|} = k_0 \sin\theta \tag{15}$$

which means in-plane component of incident wavevector matches Bloch wavevector.

Another point that can be revealed by photonic bandstructure is slow light enhancement. It can be seen from Fig. 8 that the photon group velocity is significantly lower than the phase velocity especially at bandedge such as Γ point at long wavelength portion. The group velocity characterizes the electromagnetic wave propagation in the film and it can be expressed as:

$$v_g = \frac{\partial \omega(k)}{\partial k} \tag{16}$$

The group velocity is related to the slope of photonic bandstructrue. In cavity the propagation of electromagnetic wave is no longer plane wave of infinitely extent and the photonic density of state (PDOS) is modified. Properly tailored and optimized cavity will lead to enhanced solar cell absorbance due to modified density of state and extended photon cavity lifetime.

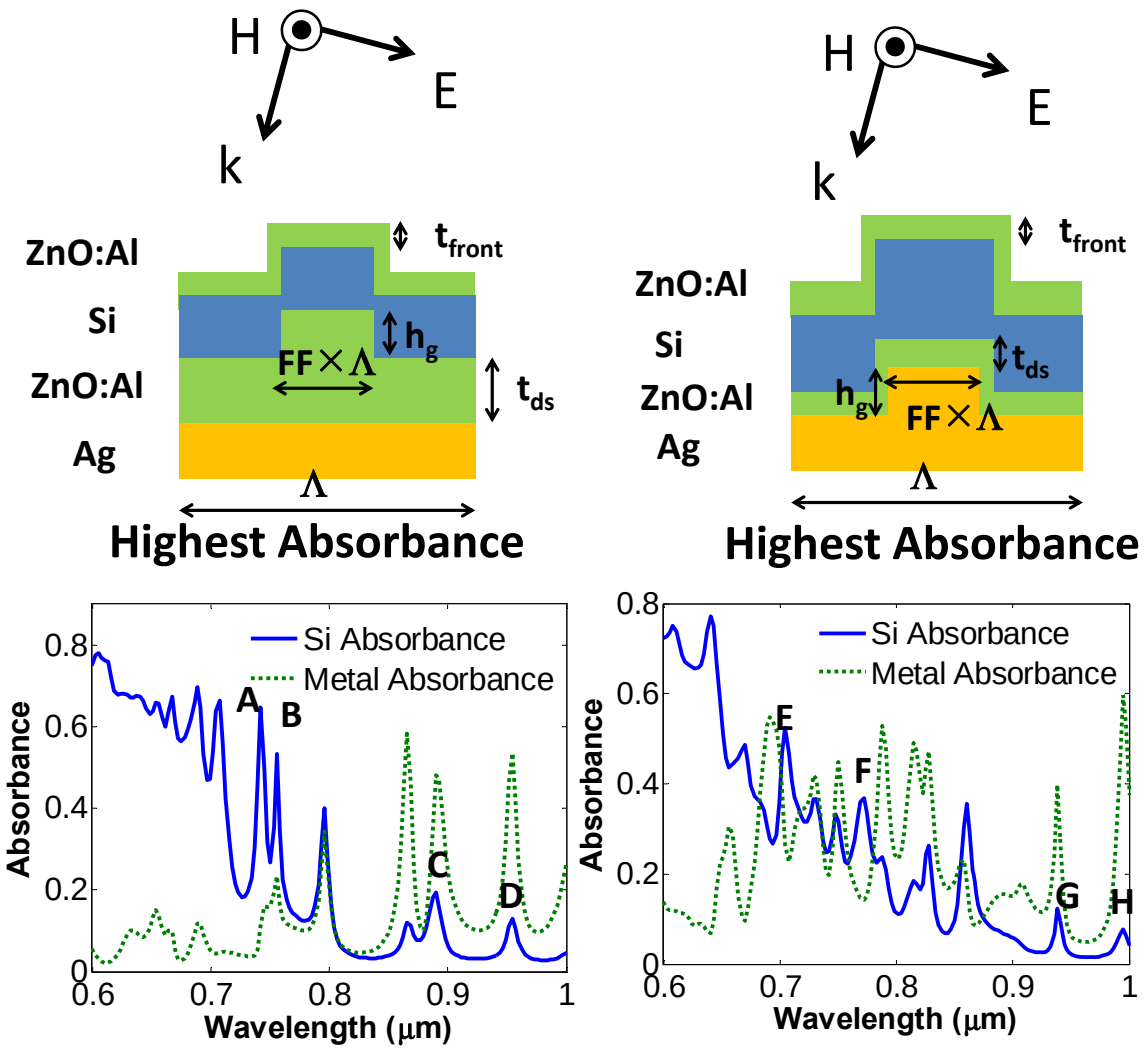

Fig. 9 The highest short circuit current spectral response for the dielectric-spaced plasmonic back reflectors after optimization for (left) the grating on the dielectric-spacer(GDS) structure and (right) the grating on the silver(GS) structure.

From previous sections, it is seen that the absorbance enhancement by the purely plasmonic back reflectors without a dielectric spacer is significantly lower than the non-plasmonic diffractive back reflectors ones due to metallic absorption. To improve the silicon absorption by reducing metallic absorption, the $J_{SC,LT}$ is now calculated for dielectric-spaced structures and the geometry optimization is carried out for the grating period(Λ), fill factor(FF), grating height(hg), incident angle(θ), and dielectric spacer thickness(t_{ds}), as illustrated in the drawing of Fig. 9. In theoretical papers, there are two types of structure exist for dielectric spaced plasmonic back reflectors[33, 42]: one is grating on the dielectric spacer(GDS) [33] and the other is grating on silver(GS) [42]. The GDS structure is illustrated on the left in Fig. 9 where the grating is etched on the dielectric spacer and the silver-dielectric spacer interface is mostly flat. The GS structure is illustrated on the right in Fig. 9 where a grating is formed on the silver surface and then a conformal dielectric spacer layer is deposited on silver. In experiment, GS structure is mostly conducted, and the practice is texturing the silver

back reflector before depositing the subsequent layers. Therefore the experimental structure is more similar to the grating on silver(GS) structure. Nonetheless, it is going to be shown that the GS structure is less efficient then the GDS structure at their respective optimized geometry, due to the lower metallic absorption of the GDS structure. For GDS structure, the optimized geometry is Λ=0.4684μm, FF=0.3548, hg=0.198μm, t_{ds}=0.144μm, and θ=7.0866°. For GS structure, the optimized geometry is Λ=0.548μm, FF=0.2471, hg=0.187μm, t_{ds}=0.25μm, and θ=4.7244°. t_{front} is fixed at 80nm for both structures. The optimized highest short circuit current at light trapping wavelength, $J_{SC,LT}$, is **7.6387 mA/cm^2 f**or the grating on dielectric spacer(GDS) structure, and **7.1617 mA/cm^2** for the grating on the silver(GS) structure, which are all higher than the case without the dielectric spacer for the purely SP back reflectors without a dielectric spacer in Section 4 ($J_{SC,LT}$=**6.3399 mA/cm^2**). The improvement in $J_{SC,LT}$ for GDS structure is 20.49%, compared to SP back reflectors without a dielectric spacer.

It should be pointed out that the number of excited quasi-guided modes also shows increase as the optimization proceeds, but the optimization still does not converge to the geometry that leads to the most supported modes. In order to keep the paper concise, the statistics for the optimization is not shown here again for the dielectric-spaced structures. Repeated global optimization run is also conducted, and similar results are arrived. Therefore, the optimized geometry giving the highest short circuit current does not coincide with the geometry leading to the most quasi-guided modes. Surface plasmons are still excited at specific wavelengths although it is of much weaker strength compared to the plasmonic back reflector without a dielectric spacer. The excitation of surface plasmons(SP) in dielectric spaced structures is due to the incomplete shielding of the dielectric. The metallic absorption is effectively reduced and the optimized trade-off between SP excitation and SP absorption leads to higher silicon absorbance. Therefore, for the plasmonic back reflectors in inorganic solar cell structures, direct contact of metal-semiconductor, such as the case in section 4, tends to result in increased metallic absorption and is not a preferable way for light trapping. While near field SP effect can be extremely effective[34, 43] in organic devices, the far field SP light scattering by SP back reflectors in inorganic semiconductor can be significantly degraded by metallic absorption. The metallic loss is especially detrimental if a whole metallic back reflector is directly in contact with the semiconductor[51], compared to the case where only small nano-scale metallic particles are placed at the front or the rear side of the devices[78]. While a lot of SP structures with metal back reflectors directly in contact with inorganic semiconductor is conducted[35, 51], it is suggested here that the conventional dielectric spaced back reflector is still more efficient for long-wavelength light trapping, due to the balance between SP assisted absorption enhancement and metallic absorption loss. Surprisingly, it is also found that the grating on the dielectric spacer(GDS) itself is more effective than the grating on the silver(GS) back reflector, different from the experimental practice were the metallic back reflectors are textured before the subsequent depositions. The higher $J_{SC,LT}$ is mainly because the GS structure tends to lead to more metallic absorption, evident from the spectral response in Fig. 9.

Since in reality the two-dimensional texture or grating is mostly used for solar cells, the excitation of surface plasmon exists for both TE and TM polarizations. It is therefore suggested that for solar cells with metal back reflectors, dielectric spacer should be included and the texture should be formed the dielectric spacer itself. In the cases where dielectric mirrors are employed, high-Q diffractive modes should be utilized to maximize the short circuit current as shown in section 3. In addition, while most of the experimental solar

cells still employ metal back reflectors, non-plasmonic back reflectors, such as dielectric mirrors, can potentially provide higher photocurrent due to lower SP absorption loss.

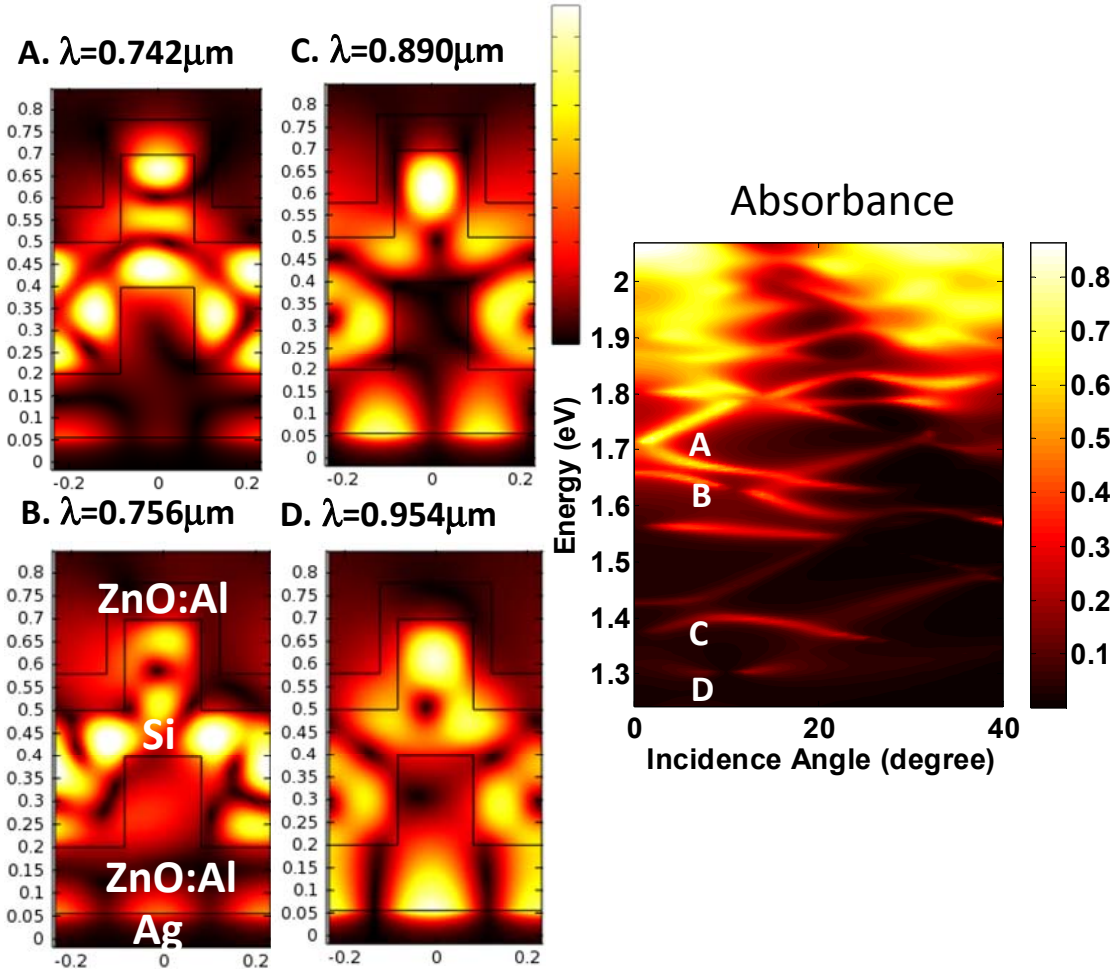

Fig. 10 (Left) the field profiles at the quasi-guided mode peak wavelengths for the optimized grating on the dielectric spacer(GDS) structure. (Right) the corresponding photonic bandstructure.

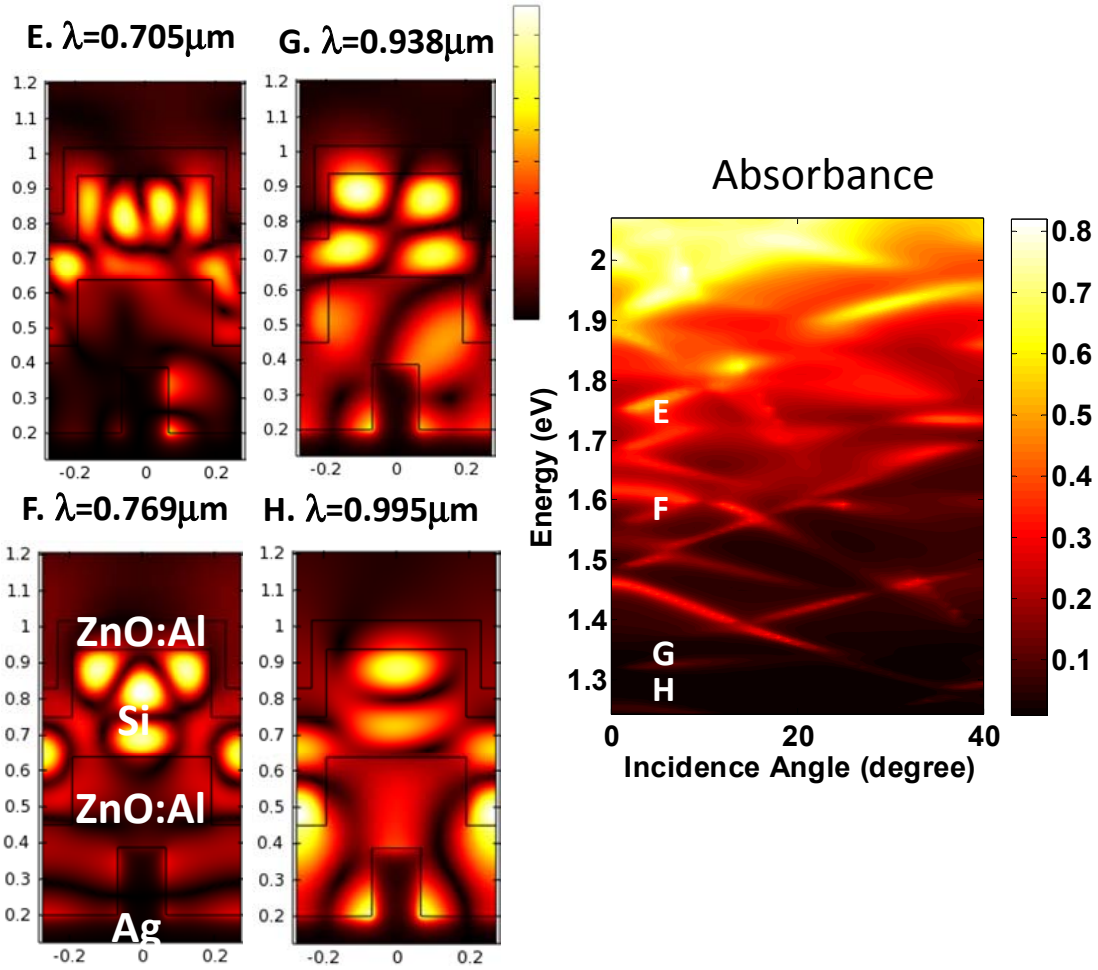

Fig. 11 (Left) the field profiles at the quasi-guided mode peak wavelengths for the optimized grating on the silver(GS) structure. (Right) the corresponding photonic bandstructure.

Fig. 10 and Fig. 11 show the field profiles and the photonic bandstructures of the optimized geometry, for both GDS and GS dielectric-spaced structures. It can be seen from Fig. 9 that in spectral responses some of the quasi-guided mode peaks are accompanied by the elevated metallic absorption while the other peaks are not. The enhanced field intensity at metal-silicon interface at the long wavelength in Fig. 10(λ=0.954μm) and Fig. 11(λ=0.995μm) further confirms the excitation of surface plasmons. The quasi-guided mode excitation is also labeled in the photonic bandstructure at the right of Fig. 10 and Fig. 11. The Bloch wavefunction for a periodic structure can generally be written as

$$\vec{E}(\vec{r},t) = \mathrm{Re}\left\{\vec{u}(\vec{r})\exp(-j\vec{k}_{Bloch}\cdot\vec{r})\exp(j\omega t)\right\} \tag{17}$$

where E is the electric field, k_{Bloch} is the Bloch wavevector, ω is angular frequency, t is the time, and u is the periodic modulation. The condition for the excitation of the qausi-guided modes is

$$k_0 \sin\theta = \omega\sqrt{\mu_0\varepsilon_0}\sin\theta = \vec{k}_{Bloch} \tag{18}$$

where k_0 is the free space wavevector of the incident field, μ_0 and ε_0 is the free space permeability and permittivity respectively, and θ is the incidence angle as illustrated in Fig. 4. It should be pointed out that here the x-axis in the photonic bandstructure is θ rather than k_{Bloch}, and the conversion between them is also established by Eq.(4).

The slope of the photonic band structure is the photon group velocity:

$$\frac{d\omega}{dk_{Bloch}} = \frac{d\omega}{d\theta}\left(\frac{dk_{Bloch}}{d\theta}\right)^{-1} = \frac{d\omega}{d\theta}\frac{1}{k_0\cos\theta} \tag{19}$$

Although the slow light enhancement is not the main point of this paper, it is still worth to point out that at the quasi-guided mode wavelengths, the photon group velocity is significantly slower than its free space phase velocity and therefore the enhanced absorbance can be achieved.

Optimized diffractive element: Random gratings

The calculation of Poynting vector, energy loss, and integrated quantum efficiency can be referred to literatures[7, 8, 26, 64]. The calculated integrated absorbance, A_{Int}, is 0.7380 for the optimized geometry and 0.5697 for its periodic counterpart. The optimized grating geometry is shown in Fig. 12. The spectral response is shown in Fig. 13 where a 4X4 quasi-random grating provides 23% broad band improvement compared to its 2D periodic counterpart. At short wavelength, the optimized structure shows broad band improvement due to the transmission enhancement, as is clear in the insect of Fig. 13. At long wavelengths, the Fabry-Perot type resonances are seen in the 2D-periodic grating due to the quasi-guided mode excitations.

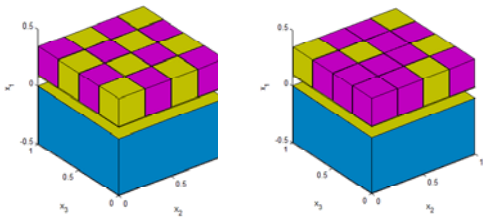

Fig. 12 (Left) periodic two-dimensional grating. (Right) optimized quasi random 4x4 grating.

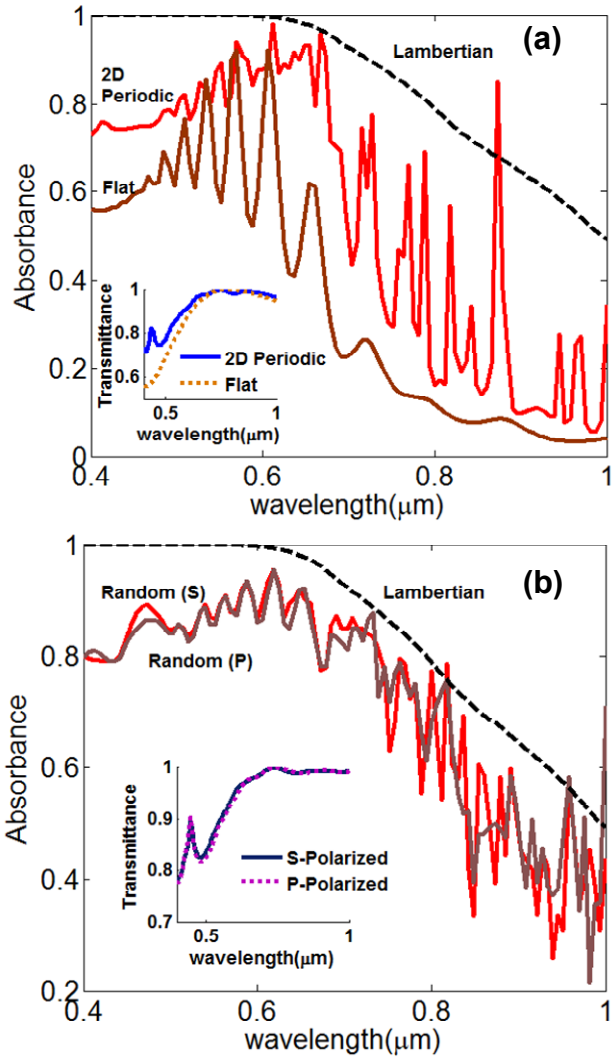

Fig. 13. Spectral responses for (a) the 2D periodic grating and (insect) the transmission at the front surface (b) the optimized 4X4 quasi-random grating and (insect) transmission at the front surface.

The Lambertian absorption limit is[79]:

$$\mathrm{A}(\lambda) = \frac{(1-e^{-4\alpha W})}{[1-(1-1/n^2)e^{-4\alpha W}]} \tag{20}$$

where α is the absorption coefficient, n is the semiconductor refractive index, and W is the film thickness. Although at the resonance frequencies the absorbance of the baseline cell with 2D periodic gratings can exceed the Lambertian limit in (6) at certain wavelengths, the broad band enhancement is not as strong as the optimized random structure. The well-defined quasi-guided-modes in the periodic grating make it possible to exceed the Lambertian limit. Nonetheless, at wavelengths other than the resonances, the absorbance is much lower. Since it is difficult for guided modes to exist over the entire solar spectrum, a comprised but optimized random grating can provide higher overall efficiency. Planar cell in general shows wave interference characteristics at the short wavelength where peaked absorbance is seen when wave impedance is matched for the thin-film solar cell stack. It shows weak absorption at long wavelength due to insufficient light scattering, resulting from the lack of large angle diffraction.

The transmission at the solar cell front surface is plotted at the insects of Fig. 13. When calculating the transmittance, only the front surface texture is retained (no back reflector) and the fraction of the power

penetrating from air into silicon is plotted. Retaining only the front surface texture is a common practice for calculating anti-reflection characteristics[35]. Since there is no back reflector, no quasi-guided mode is excited and therefore in the transmittance curve very few peaks are observed. At the long wavelength portion of the solar spectrum, the transmission is essentially very high due to the matched wave impedance. The impedance matched condition for the ZnO front contact assuming planar structure is:

$$t_{\mathrm{ZnO}} = \frac{\lambda}{4n_{\mathrm{ZnO}}} + \frac{m\lambda}{2n_{\mathrm{ZnO}}} \tag{21}$$

where λ is the free space wavelength, n_{ZnO} is the ZnO refractive index, and m is non-negative integer. For the 2D-perioidic grating the transmission is further improved at all wavelengths where a broad band transmission is observed instead of perfect transmission at a single wavelength, as is the case for the planar structure. The lower transmission at the short wavelength for both insects in Fig. 13(a)(b) is due to two factors. First is directly from (7). n_{ZnO} is approximately equal to 2 and t_{ZnO} =100nm, and thus the first impedance matched point is around λ=800nm, and the second is λ=266.67 nm. Since there is no impedance matched point around λ=400nm-600nm, the transmission is lower at short wavelength. The second reason is that the imaginary part of dielectric constant (ε_r") becomes higher at short wavelength, which in turn lowers the transmission. The transmission peak around λ=448.5nm is unlikely the result of impedance matching since there is no such points in this spectral range. It is more likely due to the strong waveguiding effect where the ridged-geometry guides the incident wave into the silicon slab. The further broad band transmission improvement of the random grating over the 2D periodic grating is due to its optimized geometry.

[1] H. Sai*, et al.*, "Light trapping effect of submicron surface textures in crystalline Si Solar Cells," *Prog. Photovolt. Res. Appl.,* vol. 15, pp. 415–423, 2007.

[2] S.-S. Lo*, et al.*, "Broad-band anti-reflection coupler for a : Si thin-film solar cell," *J. Phys. D: Appl. Phys. ,* vol. 40, pp. 754–758 2007.

[3] C. Haase and H. Stiebig, "Thin-film silicon solar cells with efficient periodic light trapping texture," *Appl. Phys. Lett.,* vol. 91, p. 061116, 2007.

[4] H. Stiebig*, et al.*, "Silicon thin-film solar cells with rectangular-shaped grating couplers," *Prog. Photovolt. Res. Appl.,* vol. 14, pp. 13–24, 2006.

[5] H. Stiebig*, et al.*, "Light trapping in thin-film silicon solar cells by nano-textured interfaces," in *Photonics for Solar Energy Systems*, Strasbourg, France, 2006, p. 619701.

[6] C. Haase and H. Stiebig, "Optical properties of thin-film silicon solar cells with grating couplers, design and fabrication of submicron grating structures for light trapping in silicon solar cells," *Prog. Photovolt. Res. Appl. ,* vol. 14, pp. 629–641, 2006.

[7] P. Bhattacharya, *Semiconductor Optoelectronic Devices, 2nd Ed.* Upper Saddle River, NJ: Prentice-Hall, 2006.

[8] Synopsys, "Sentaurus Device EMW User Manual V. X-2005.10," ed, 2005, pp. 78-79.

[9] V. Shah*, et al.*, "Thin-film silicon solar cell technology," *Prog. Photovolt. Res. Appl. ,* vol. 12, pp. 113–142 2004.

[10] N. Senoussaoui*, et al.*, "Thin-film solar cells with periodic grating coupler," *Thin Solid Films* vol. 451–452 pp. 397–401, 2004.

[11] J. Krc*, et al.*, "Potential of light trapping in microcrystalline silicon solar cells with textured substrates," *Prog. Photovolt. Res. Appl.,* vol. 11, pp. 429–436, 2003.

[12] S. S. Hegedus and R. Kaplan, "Analysis of quantum efficiency and optical enhancement in amorphous Si p–i–n solar cells," *Prog. Photovolt. Res. Appl. ,* vol. 10, pp. 257–269 2002.

[13] T. Brammer*, et al.*, "Optical properties of silicon-based thin-film solar cells in substrate and superstrate configuration," *Sol. Energ. Mat. Sol.,* vol. 74, pp. 469– 478, 2002.

[14] A. Shah*, et al.*, "Photovoltaic technology: the case for thin-film solar cells," *Science,* vol. 285, pp. 692-698, 1999.

[15] M. T. Gale*, et al.*, "Design and fabrication of submicron grating structures for light trapping in silicon solar cells," in *Proceedings of SPIE, Conference on Optical Materials Technology for Energy Efficiency and Solar Energy Conversion IX*, 1990, pp. 60-66.

[16] C. F. R. Mateus*, et al.*, "Ultrabroadband mirror using low-index cladded subwavelength grating," *IEEE Photon. Tech. Lett.,* vol. 16, pp. 518-520, 2004.

[17] R. Magnusson and M. Shokooh-Saremi, "Physical basis for wideband resonant reflectors," *Optics Express,* vol. 16, pp. 2456-3462, 2008.

[18] M. C. Y. Huang*, et al.*, "A nanoelectromechanical tunable laser," *Nature Photonics,* vol. 2, pp. 180-184, 2008.

[19] X. M. Zhang*, et al.*, "Variable nano-grating for tunable filters," in *The 14th International Conference on Solid-State Sensors, Actuators and Microsystems*, Lyon, France, 2007, pp. 2417-2420.

[20] M. C. Y. Huang*, et al.*, "A surface-emitting laser incorporating ahigh-index-contrast subwavelength grating," *Nature Photonics,* vol. 1, pp. 119-122, 2007.

[21] S. Boutami*, et al.*, "Broadband and compact 2-D photonic crystal reflectors with controllable polarization dependence," *IEEE Photon. Tech. Lett.,* vol. 18, pp. 835-837, 2006.

[22] Schokley and Queisser, "Detailed balance limit of efficiency of p-n junction solar cell," *J. Appl. Phys.,* vol. 32, pp. 510-519, 1961.

[23] R. R. King*, et al.*, "40% efficient metamorphic GaInP/GaInAs/Ge multijunction solar cells," *Applied Physics Letter,* vol. 90, p. 183516, 2007.

[24] D. Cheyns*, et al.*, "The angular response of ultrathin film organic solar cells," *Appl. Phys. Lett.,* vol. 92, p. 243310, 2008.

[25] K. Knop, "Reflection grating polarizer for the Infrared," *Opt. Commun.,* vol. 26, pp. 281-283, 1978.

[26] A. Lin and J. D. Phillips, "Optimization of random diffraction gratings in thin-film solar cells using genetic algorithms," *Sol. Energ. Mat. Sol.,* vol. 92, pp. 1689-1696, 2008.

[27] A. Meyer and H. Adea, "The effect of angle of incidence on the optical field distribution within thin film organic solar cells," *J. Appl. Phys.,* vol. 106, p. 113101, 2009.

[28] W. E. I. Sha*, et al.*, "Angular response of thin-film organic solar cells with periodic metal back nanostrips," *Opt. Lett.,* vol. 36, pp. 478-480, 2011.

[29] M. Yang*, et al.*, "Incident angle dependence of absorption enhancement in plasmonic solar cells," *Opt. Express,* vol. 19, pp. A763-A771, 2011.

[30] Z. Yu and S. Fan, "Angular constraint on light-trapping absorption enhancement in solar cells," *Applied Physics Letter,* vol. 98, p. 011106, 2011.

[31] S. B. Mallick*, et al.*, "Optimal light trapping in ultra-thin photonic crystal crystalline silicon solar cells," *Optics Express,* vol. 18, pp. 5691-5706, 2010.

[32] B.-J. Kim and J. Kim, "Fabrication of GaAs subwavelength structure (SWS) for solar cell applications," *Optics Express,* vol. 19, pp. A326-A330, 2011.

[33] X. Sheng*, et al.*, "Optimization-based design of surface textures for thin-film Si solar cells," *Optics Express,* vol. 19, pp.

A841-A850, 2011.

[34] K. Q. Le, *et al.*, "Comparing plasmonic and dielectric gratings for absorption enhancement in thin-film organic solar cells," *Opt. Express,* vol. 20, pp. A39-A50, 2012.

[35] U. W. Paetzold, *et al.*, "Design of nanostructured plasmonic back contacts for thin-film silicon solar cells," *Opt. Express,* vol. 19, pp. A1219-A1230, 2011.

[36] U. W. Paetzold, *et al.*, "Plasmonic reflection grating back contacts for microcrystalline silicon solar cells," *Appl. Phys. Lett.,* vol. 99, p. 181105, 2011.

[37] J. N. Munday and H. A. Atwater, "Large Integrated Absorption Enhancement in Plasmonic Solar Cells by Combining Metallic Gratings and Antireflection Coatings," *Nano Lett.,* vol. 11, pp. 2195–2201, 2011.

[38] N. Lagos, *et al.*, "Theory of plasmonic near-field enhanced absorption in solar cells," *Appl. Phys. Lett.,* vol. 99, p. 063304, 2011.

[39] F.-J. Haug, *et al.*, "Resonances and absorption enhancement in thin film silicon solar cells with periodic interface texture," *J. Appl. Phys.,* vol. 109, p. 084516, 2011.

[40] F. J. Beck, *et al.*, "Light trapping with plasmonic particles: beyond the dipole model," *Opt. Express,* vol. 19, pp. 25230-25241, 2011.

[41] S. Zanotto, *et al.*, "Light trapping regimes in thin-film silicon solar cells with a photonic pattern," *Opt. Express,* vol. 18, pp. 4260-4274, 2010.

[42] K. Söderström, *et al.*, "Photocurrent increase in n-i-p thin film silicon solar cells by guided mode excitation via grating coupler," *Appl. Phys. Lett.,* vol. 96, p. 213508, 2010.

[43] C. Min, *et al.*, "Enhancement of optical absorption in thin-film organic solar cells through the excitation of plasmonic modes in metallic gratings," *Appl. Phys. Lett.,* vol. 96, p. 133302, 2010.

[44] F. J. Beck, *et al.*, "Asymmetry in photocurrent enhancement by plasmonic nanoparticle arrays located on the front or on the rear of solar cells," *Appl. Phys. Lett.,* vol. 96, p. 033113, 2010.

[45] H. A. Atwater and A. Polman, "Plasmonics for improved photovoltaic devices," *Nature Mater.,* vol. 9, pp. 205-213, 2010.

[46] P. N. Saeta, *et al.*, "How much can guided modes enhance absorption in thin solar cells," *Opt. Express,* vol. 17, pp. 20975-20990, 2009.

[47] W. Bai, *et al.*, "Design of plasmonic back structures for efficiency enhancement of thin-film amorphous Si solar cells," *Opt. Lett.,* vol. 34, pp. 3725-3727, 2009.

[48] K. R. Catchpole and A. Polman, "Plasmonic solar cells," *Opt. Express,* vol. 16, pp. 21793-21800, 2008.

[49] V. E. Ferry, *et al.*, "Light trapping in ultrathin plasmonic solar cells," *Opt. Express,* vol. 18, pp. A237-A245, 2010.

[50] A. Lin, *et al.*, "An optimized surface plasmon photovoltaic structure using energy transfer between discrete nano-particles," *Opt. Express,* vol. 21, pp. A131-A145 2013.

[51] H.-Y. Lin, *et al.*, "Surface plasmon effects in the absorption enhancements of amorphous silicon solar cells with periodical metal nanowall and nanopillar structures," *Opt. Express,* vol. 20, pp. A104-A118, 2012.

[52] S. Pillai, *et al.*, "The effect of dielectric spacer thickness on surface plasmon enhanced solar cells for front and rear side depositions," *J. Appl. Phys.,* vol. 109, p. 073105, 2011.

[53] C. Battaglia, *et al.*, "Light trapping in solar cells: can periodic beat random?," *ACS Nano.,* vol. 6, pp. 2790-2797, 2012.

[54] Z. Yu, *et al.*, "Fundamental limit of light trapping in grating structures," *Opt. Express,* vol. 18, pp. A366-A380, 2010.

[55] S. Pillai and M.A.Green, "Plasmonics for photovoltaic applications," *Sol. Energ. Mat. Sol.,* vol. 94, pp. 1481–1486, 2010.

[56] Z. Yu, *et al.*, "Fundamental limit of nanophotonic light trapping in solar cells," *Proc. Natl. Acad. Sci. USA,* vol. 107, pp.

17491-17496, 2010.

[57] D. E. Goldberg, *Genetic Algorithms in Search, Optimization, and Machine Learning*, 1 ed.: Addison-Wesley Professional, 1989.

[58] E. Yablonovitch, "Statistical Ray Optics," *J. Opt. Soc. Am.,* vol. 72, pp. 899-907, 1982.

[59] V. Ganapati*, et al.*, "Spontaneous Symmetry Breaking in the Optimization of Subwavelength Solar Cell Textures for Light Trapping," in *IEEE Photovoltaic Specilist Conference*, Austin, USA, 2012.

[60] C. Munuera*, et al.*, "Morphology of ZnO grown by MOCVD on sapphire substrates," *J. Cryst. Growth,* vol. 264, pp. 70-78, 2004.

[61] T. Söderström*, et al.*, "Optimization of amorphous silicon thin film solar cells for flexible photovoltaics," *J. Appl. Phys.,* vol. 103, p. 114509, 2008.

[62] M. A. Green*, et al.*, "Solar cell efficiency tables (Version 29)," *Prog. Photovolt. Res. Appl.,* vol. 15, pp. 35 –40, 2007.

[63] A. Lin*, et al.*, "Lithographically-definable Solar Cell Random Reflector using Genetic Algorithm Optimization," in *IEEE Photovoltaic Specilist Conference*, Austin, USA, 2012.

[64] C. AB, *Comsol Multiphysics RF Module User Guide V 3.3*, 2006.

[65] B. Deken*, et al.*, "Minimization of field enhancement in multilayer capacitors," *Computational Mater. Sci. ,* vol. 37, pp. 401–409, 2006.

[66] S. Preblea*, et al.*, "Two-dimensional photonic crystals designed by evolutionary algorithms," *Appl. Phys. Lett.,* vol. 86, pp. 061111-1-061111-3, 2005.

[67] L. Shen*, et al.*, "Design of two-dimensional photonic crystals with large absolute band gaps using a genetic algorithm," *Phy s. Rev. B,* vol. 68, pp. 035109-1-035109-5, 2003.

[68] H. Lipson and J. B. Pollack, "Automatic design and manufacture of robotic lifeforms," *Nature,* vol. 406, pp. 974-978, 2000.

[69] Rsoft, *Rsoft CAD User Manual*, 8.2 ed. New York: Rsoft Design Group, 2010.

[70] M. E. Fragala*, et al.*, "Structural, Optical, and Electrical Characterization of ZnO and Al-doped ZnO Thin Films Deposited by MOCVD," *Chem. Vap. Deposition,* vol. 15, pp. 327-333, 2009.

[71] J. W. Elam*, et al.*, "Properties of ZnO/Al2O3 Alloy Films Grown Using Atomic Layer Deposition Techniques," *J. Electrochem. Soc.,* vol. 150, pp. G339-G347, 2003.

[72] H. Kim*, et al.*, "Effect of aluminum doping on zinc oxide thin films grown by pulsed laser deposition for organic light-emitting devices," *Thin Solid Film,* vol. 377-378, pp. 798-802, 2000.

[73] J. M. Khoshman and M. E. Kordesch, "Optical constants and band edge of amorphous zinc oxide thin films," *Thin Solid Films* vol. 515, pp. 7393–7399, 2007.

[74] S. J. Kang and Y. H. Joung, "Influence of substrate temperature on the optical and piezoelectric properties of ZnO thin films deposited by rf magnetron sputtering," *Appl. Surf. Sci. ,* vol. 253, pp. 7330–7335, 2007.

[75] A. S. Ferlauto*, et al.*, "Analytical model for the optical functions of amorphous semiconductors and its applications for thin film solar cells," *Thin Solid Films* vol. 455 –456 pp. 388–392, 2004.

[76] O. S. o. America, *Handbook of optics, vol. 2: devices, measurements, and properties, second edition* vol. 2: McGraw-Hill Professional, 1994.

[77] H. Kima*, et al.*, "Effect of aluminum doping on zinc oxide thin films grown by pulsed laser deposition for organic light-emitting devices," *Thin Solid Film,* vol. 377-378, pp. 798-802, 2000.

[78] S. Pillai*, et al.*, "The effect of dielectric spacer thickness on surface plasmon enhanced solar cells for front and rear side depositions," *J. Appl. Phys.,* vol. 109, p. 073105, 2011.

[79] M. A. Green, "Lambertian Light Trappingin Textured Solar Cells and Light-Emitting Diodes: Analytical Solutions," *Prog. Photovolt: Res. Appl.,* vol. 10, pp. 235-241, 2002.

國科會補助專題研究計畫項下出席國際學術會議心得報告

日期：101 年 12 30 日

計畫編號	NSC 101-2218-E-009-001-		
計畫名稱	以光場增強效應提升薄膜太陽能電池吸收效率研究		
出國人員 姓名	林詩淳	服務機構 及職稱	交通大學 電子工程學系
會議時間	101 年 6 月 2 日至 101 年 6 月 8 日	會議地點	Austin, TX, USA
會議名稱	（中文）**國際電機電子 38th 光伏打專家會議** （英文） IEEE 38th Photovoltaic Specialist Conference		
發表論文 題目	（中文）太陽能隨機底部反射鏡之最佳化運用基因演算法 （英文）Optimization of solar cell random reflector using genetic Algorithm		

報告內容應包括下列各項：

一、 參加經過

第一天

論文發表 Poster Presentation (A unified mathematical framework for intermediate band solar cell 中間能帶太陽能電池數學模擬模型研究) 在壁報展示期間 有多位國際學者參與討論 包括 西班牙的 Antonio Marti 和來自 National Renewable Energy Lab(美國國家再生能源實驗室), 香港理工大學和中國大陸之與會人士

聆聽演講

將第一天重要演講內容紀錄如下

由 United Solar Inc. 演講之薄膜矽多接面太陽能電池之最新發展

矽奈米太陽能電池之光場增益技術近之期發展

Advances in Light Trapping for Hydrogenated Nanocrystalline Silicon Solar Cells, *United Solar Ovonic LLC, Troy, MI, United States*

United Solar Inc 表示，對於氫化奈米矽（NC-Si：H）的太陽能電池，有紋路的背面反射鏡（BR）通常用來實現光捕獲。他們提出了氫化奈米矽（NC-Si：H）的太陽能電池銀/氧化鋅背面反射鏡的最新進展。首先，United Solar Inc 研究背面反射鏡的銀材質紋路對於氫化奈米矽（NC-Si：H）太陽能電池之光學特性的影響。United Solar Inc 調查了銀紋理的範圍很廣，而在研究中氧化鋅的厚度保持在 110-130 nm。他們觀察到，進一步加大銀質感，有效地提高光散射，但卻不增加電流密度。United Solar Inc 發現，銀/氧化鋅的結構與銀質感（RMS 約為 40 nm）和薄氧化鋅的組合提供了最高的 NC-Si：H 太陽能電池的效率。

OM&T 接著演講運用奈米壓印技術製作薄膜太陽能電池光子捕獲增強結構

第五代光場增益量產工具

Gen5 Production Tool for Light Management Textures, *OM&T B.V. / Moser Baer Technologies, Eindhoven, Netherland*

OM&T 表示光場增強正成為越來越重要的太陽能電池研究議題。 OM&T 公司摩斯巴爾技術正在探索大量低成本製造光場增強結構的可能性。在玻璃上使用奈米印跡(Nano-Imprint)的紋理，以使得最大限度的太陽光通過太陽能電池組件。OM&T 早先進行的調查表明，使用這種優化的定期紋理可以導致 10-20%的電流增益。這樣的工具可以用來生產優化紋理薄膜矽太陽能電池的 1 至 2 平方米的大型玻璃 Superstrate 太陽能電池。

第二天 聆聽演講

將第二天重要演講內容紀錄如下

Berkeley 和 LBNL 演講基礎熱力學轉換效率極限

突破太陽能電池效率之光電物理

The Opto-Electronic Physics That Broke the Efficiency Limit in Solar Cells, *Material Sciences Division, Lawrence Berkeley National Laboratory, Berkeley, CA, United States, University of California, Berkeley, Dept. of Electrical Engineering & Computer Science, Berkeley, CA, United States, National Renewable Energy Laboratory, Golden, CO, United States*

他們表示當接近根本的 Shockley -Queisser 限制時，一個太陽能電池內部物理會有所改變。光子設計的考量將超越電子的，激烈的內部和外部的發光效率需要仔細的光子管理。反直觀的說，最大限度地提高光提取效率可以提高電壓，因此。一個太陽條件下，直到 2010 年單交面 GaAs 太陽能電池的效率紀錄為 26.4%， V_{OC}= 1.03 V。Alta Devices 突破這一紀錄，達到 28.8%效率，和 V_{OC}=1.12V，這證明光子管理的重要性。即使是用最好的材料，也不一定能達到最高的效率，除非太陽能電池的設計使其也是一個很好的發光二極管 (LED)。在下一代高效率太陽能電池，光提取(light extraction)物理將是必要的

接著 U of Oklahoma & Sandia 演講運用超級晶格結構吸收太陽輻射中的紅外光

能帶中接續結構之中波段紅外光元件

Mid-IR Photovoltaic Devices Based on Interband Cascade Structures, *School of Electrical and Computer Engineering, University of Oklahoma, Norman, OK, United States, Homer L. Dodge Department of Physics and Astronomy, Norman, OK, United States, Sandia National Laboratories, Albuquerque, NM, United States*

此一演講主要是在報告光伏 (PV) 元件應用帶間級聯 (IC) 的結構設計和實施的進度。這些設備的設計，增強的電子屏障和 p 型砷化銦/銻化鎵超晶格(superlattice)吸收層。這些功能已被證明是能成功的抑制探測器的暗電流。他們的七個階段的元件，在 80 K 和 300 K 的截止波長為 4.0 微米和 5.0 微米。在低溫下觀察具良好的光響應和暗電流抑制。 在 1200K 黑體輻射之照射下和 80 K 的器件溫度條件，短路電流為 5.46 mA/cm2，開路電壓為 1.61V。當溫度為 80 K 以上，光照下，U of Oklahoma 能夠觀察到的高值開路電壓一直到 140 K。

第三天

將第三天重要演講內容紀錄如下

聆聽演講

Arizona State University 演講熱載子太陽能電池的模擬

Simulation of Carrier Relaxation in Hot-Carrier Solar Cells , *Arizona State University, Tempe, AZ, United States*

ASU 的學者表示，熱載流子的太陽能電池嚴格依賴於吸收材料中之光生載流子能量弛豫動力學，其中熱載流子通過能量選擇性接面而被提取。在這裡，他們用與能量平衡方程方法相結合的綜蒙特卡羅（EMC）去仿真模擬半導體量子阱（QW）的熱載流子的太陽能電池結構下微觀載流子弛豫過程和相應的電子和電子電洞溫度，在瞬態和穩態照明的條件下。 EMC 的程式模擬光生電子和電洞的在量子局限 III-V 族多量子阱結構的動態，透過一個 Schrodinger 和 Poisson 自我一致求解的解決方案。散射過程包括由於光學聲子（極性和非極性），電子-電子在屏蔽的多子能帶散射（或是電洞-電洞，電子-電洞）。在此一研究中包括了非平衡光學聲子。

Purdue 和 U. of Washington 的教授報告修正熱力學極限的實用極限
Shockley-Queisser 極限和現實的轉換效率極限
The Shockley-Queisser Limit and Practical Limits of Nanostructured Photovoltaics, *Purdue University , West Lafayette, IN, United StatesUniversity of Washington, Seattle, WA, United States*

在這裡，Purdue Univ. & U. of Washington 發表：(1) 討論所謂的 Shockley-Queisser 轉換效率極限和用來計算它的假設條件 (2) 通過修改詳細的平衡計算，包括 Shockley-Read-Hall 材料中和接面複合，提出新的和簡單的模型去計算奈米光伏照明的實際轉換效率極限。一般來說“Shockley-Queisser 極限”為一個理想之單一能隙太陽能電池的轉換效率極限。然而，取決於選用的太陽能頻譜和背面折射指數，(後者的意義，尤其是低估)，結果將有巨大的變化。他們發現，最合理的轉換效率極限值與原來報告的 Shockley-Queisser 顯著不同，他們也報告了當前最高記錄的光伏設備相對於 Shockley-Queisser 轉換效率極限的差異，並研究 *FF*, J_{SC}, V_{OC}, 的實際和理論極限值的不同。此外，提出一種新的模式，構建了詳細的平衡限制，特別是在計算實用轉換效率極限與奈米器件的特徵尺寸的關係。他們假設一個平均的過剩少數載流子並包括 Shockley-Read-Hall 整體合接面複合來計算暗電流。光電流計算，使用過境時間模型。他們能夠廣泛的估計半導體 V_{OC}，J_{SC} 和 η 不論元件參數為何。他們的結果強調了長的少數載流子的壽命，低界面複合速度，和雜質參雜控制的重要以實現 MEG 的利益。

第四天

將第四天重要活動內容紀錄如下

我自己的論文發表

論文發表 Oral Presentation (Optimization of solar cell random reflector using genetic Algorithm 對於隨機幾何太陽能電池底部反射鏡之最佳化)

聆聽演講

大規模奈米線薄膜太陽能電池之模擬與製造
Fabrication and Modeling of Large-Scale Silicon Nanowire Solar Cells for Thin-Film Photovoltaics
Department of Photonic & Institute of Electro-Optical Engineering, National Chiao Tung University, Hsinchu, Taiwan, Graduate Institute of Photonics and Optoelectronics, National Taiwan University, Taipei, Taiwan

交大光電的研究團隊，表示由於降低了材料的使用和晶圓質量限制，奈米晶體矽薄膜太陽能電池十分

的有潛力。在這項研究中，提出了一個簡單和符合成本效益的方法，採用聚苯乙烯奈米球光刻和金屬輔助化學蝕刻（MACE）生產各種長度的大面積矽奈米線（矽奈米線）陣列，。奈米線的結構具有寬帶和全方位的抗反射性，最低的 AM1.5G 頻譜加權矽奈米線陣列的反射率是 4.38%，比傳統的單層防反射塗層（SLARC）的 8.84%。下一步，他們將太陽能電池結合矽奈米線陣列結構，其電源效率達到 10.8%。之後透過外部和內部量子效率測量，他們對矽奈米線陣列太陽能電池的性能進行分析，他們發現直接和間接的界面載子複合式效率轉換的最大限制。他們進一步發展基於三維（3D）光學和二維（2D）量身定制的奈米矽光伏器件的電氣模擬建模技術。光學模擬採用了嚴格的耦合波分析（RCWA）技術，計算電磁場分佈，以獲得在奈米結構中的電子電洞對生成率。下一步，電氣計算是基於二維自我一致漂移擴散和泊松方程式使用有限元素法（FEM）求解。他們調查在三種不同的結構中載流子擴散長度對奈米晶體矽薄膜太陽能電池性能的影響。仿真結果表明，短的擴散長度不嚴重惡化的核殼(core-shell)PN 接面太陽能電池的短路電流密度和功率轉換效率，相較於傳統的平面結構。他們的工作表明，矽奈米線太陽能電池，相比於傳統的技術，可以實現高效的捕光效益和較低的材料品質要求，這將是矽薄膜太陽能電池的前景。

第五天

第五天是研討會最後一天

主要是聆聽交大余教授之 invited talk，關於防反射層之研究

聆聽演講（光伏之基礎與新概念:光捕獲與集中 Fundamental and new concepts for light concentration and light trapping)

對於 InGaP/InGaAs/Ge 三接面太陽能電池之防反射層之理論與製作運用 TiO_2 仿生結構

Antireflective Scheme for InGaP/InGaAs/Ge Triple-Junction Solar Cells based on TiO_2 Biomimetic Structures , *Department of Photonics and Institute of Electro-Optical Engineering, National Chiao Tung University, Hsinchu, Taiwan, Arima Photovoltaic & Optical Corp, Taoyuan, Taiwan*

他們表示，隨著磊晶成長的技術成熟和廉價的集中器的優勢，III-V 族多接面太陽能電池具有地面光伏應用的巨大潛力。近日，多接面太陽能電池的功率轉換效率可達到～32%，下一個太陽光照，這在所有類型的太陽能電池中的性能是最高的。由於 III-V 族多接面太陽能電池的廣泛吸收範圍，抗反射起著重要的作用，這是由於在空氣/半導體界面的顯著光損失。一個精心設計的防反光結構可以增加光子收集，以產生更多的電流密度，從而導致更高的電源轉換效率。然而，反射損耗量是與半導體和空氣折射率差有關，這是抗反射設計的關鍵，目標是消除介質環境折射率的突然變化。仿生結構，抑制菲涅爾(Fresnel)反射，由於其分級結構的分布，統稱為光子的功能梯度折射率介質。然而，在奈米結構製作的材料應該密切匹配半導體的折射率，以獲取寬帶穿透增益。在這項工作中，他們建議使用～2.4-2.6 折射率的二氧化鈦製作仿生奈米結構與單層抗反射（SL ARC）來做比較。他們還優化三接面太陽能電池厚的二氧化鈦 SLARC 厚度。初步結果表明， SLARC 與仿生奈米結構太陽能電池的表現相當的光電特性，然而二氧化鈦奈米材料的尺寸可以進一步優化。因此，一個全面的設計方案還調整了多接面電池的反射光譜以獲得最大光電流輸出。

二、 心得（可含照片）

從這一次會議學習到許多關於太陽能電池的新知識，包括

- ✓ 薄膜太陽能電池的光子捕獲和前瞻光子管理技術(thin-film solar cell light trapping, advanced photon management）包括了，防反射層之理論與實作，週期性光柵之模擬與製造，和其在薄膜太陽能電池上之應用。
- ✓ 各式太陽能電池之最新發展(current development of various solar cell technology)，包括

了 II-VI 薄膜，III-V 多接面太陽能電池，和矽薄膜。

- ✓ 未來太陽能電池技術之新概念和實踐 new concepts and practice for future high efficiency solar cell, 包括熱力學極限 實用模型和光學特性模擬。
- ✓ 多接面太陽能電池包括材料生長和電流匹配(multi-junction cell including material growth and current matching)。
- ✓ 矽晶太陽能電池之材料與元件設計考量(feedstock of c-Si solar cell)，還有奈米結構之製作與前瞻性。

從這一次會議引發了許多研究之新方向

- ✓ 銅銦鎵硒/銅鋅錫硫(CIGS/CZST) 太陽能電池
- ✓ 光子晶體太陽能電池提升光子生命週期
- ✓ 傳統矽晶太陽電池之新發展
- ✓ 熱力學極限之研究
- ✓ 漸變式折射率防反射層

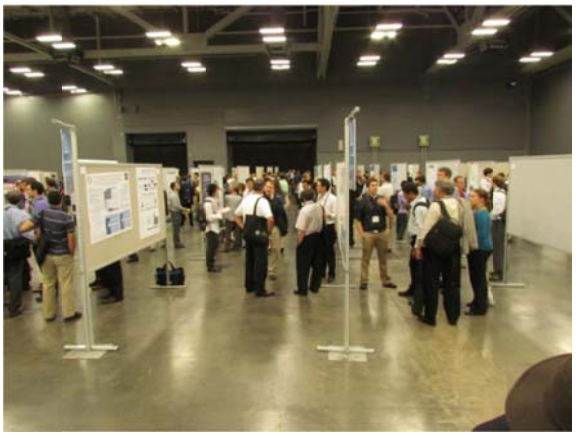

三、**考察參觀活動**(無是項活動者，或前已敘述者可省略此項)

四、 建議

暫時無建議

五、 攜回資料名稱及內容

38 屆國際電機電子協會 光伏打專家研討會 研討會論文集

Proceeding of 38th IEEE Photovoltaic Specialist Conference

多本關於光伏打最新發展之雜誌與文獻

Miscellaneous Magazines for PV

六、 其他

感謝國科會和交大研發處的支持 才能順利參與國際會議

Lithographically-definable Solar Cell Random Reflector using Genetic Algorithm Optimization

Albert S. Lin[1], Sze-Ming Fu[1], Yan-Kai Zhong[2]

[1] Institute of Electronic Engineering, National Chiao-Tung University, Hsinchu, Taiwan 30010

[2] Department of Electro-Physics, National Chiao-Tung University, Hsinchu, Taiwan 30010

***Abstract* — Randomly textured Lambertian surface provides broad band cosine emission and thus is suitable for photovoltaic application. Nonetheless, variation of efficiency and non-optimized nature of randomly textured devices are undesirable. Here it is shown that using genetic algorithm, a 4x4 binary quasi-random grating can provide 23% higher absorption than 2D periodic grating and 103.5% higher than planar cells, approaching Lambertian limit. The improvement is attributed to broad band transmission for high energy photon and broad band waveguiding effect for low energy photons. Large scale fully-optimized binary grating can potentially surpass Lambertian limit due to its optimized nature and should be employed for future thin-film photovoltaic devices to reduce film thickness and cost.**

***Index Terms* — genetic algorithm, randomized pattern, guided mode, thin-film solar cell.**

I. Introduction

Randomly textured surface provides broad band cosine emission and thus lead to so-called Lambertian limit[1]. Experimental and theoretical works have shown the superior absorption enhancement using random Lambertian surface for solar cell back or front surfaces[2-9]. Nonetheless, in order to further improve the diffraction capability of randomly textured surface and thus increase the conversion efficiency[10], optimization is essential. In addition, the geometry variation in randomly textured surfaces due to process conditions or its own randomness nature causes poor reproducibility in these devices. Previously optimization of random reflectors has been applied to 1D-profiles as in [11, 12]. In order to achieve lithographically definable random reflectors, 2D-profile optimization is necessary.

II. Evolution of Random Structures

Structure consists of ZnO/Si/ZnO/Ag, and the thickness of silicon is 700nm.The Ag and ZnO layers are firstly defined, which are uniform stratums. Then an initial binary mask pattern is defined as an array of 1 and 0. 1 represents the mesa and 0 represents the etched area, and thus 1 represents ZnO while 0 represents silicon since the etched region will be conformally filled with silicon. Afterward, a uniform stratum of silicon is defined, the thickness will be the total thickness minus the groove depth of the grating. The fifth layer is again ZnO/Silicon bi-periodic stratum, and the initial binary mask can be used to define this ZnO top contact conformal coverage. The sixth layer, which is the sidewall of the top silicon grating structure, is more complicated to define. As illustrated by Fig. 1, the side wall definition can be done by dividing the empty (air) region into 9 sub-regions, and whether each sub-region should be air or ZnO is determined by whether the adjacent region is silicon or air. The last stratum is the topmost ZnO coverage, which constitutes part of the top ZnO conformal coverage. Material optical constants can be found in literature[8, 13-16].

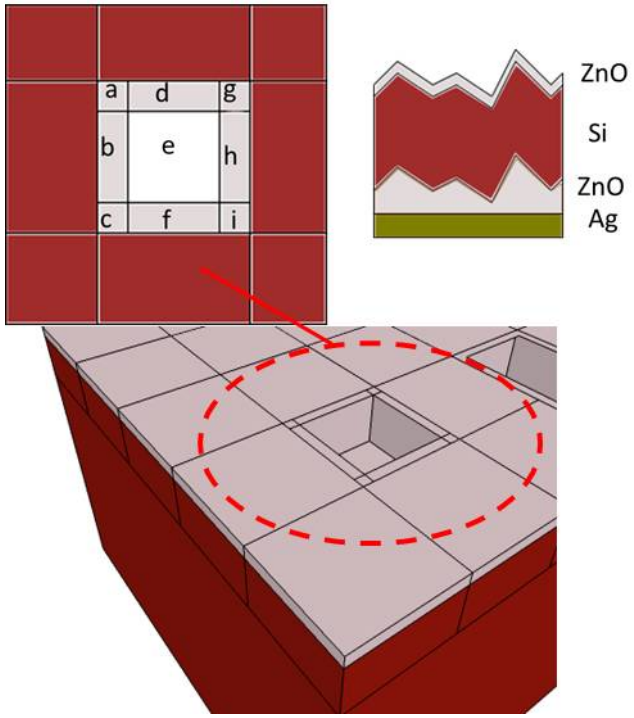

Fig. 1. Illustration the device structures and the way to define top ZnO coverage.

Genetic algorithm (GA) is applied to conduct geometry optimization for random reflectors. GA has been shown to be successful in several different engineering fields[17-21]. It is a global optimization technique mimicking the process of

nature evolution. The structure for evolution is shown in Fig. 2.

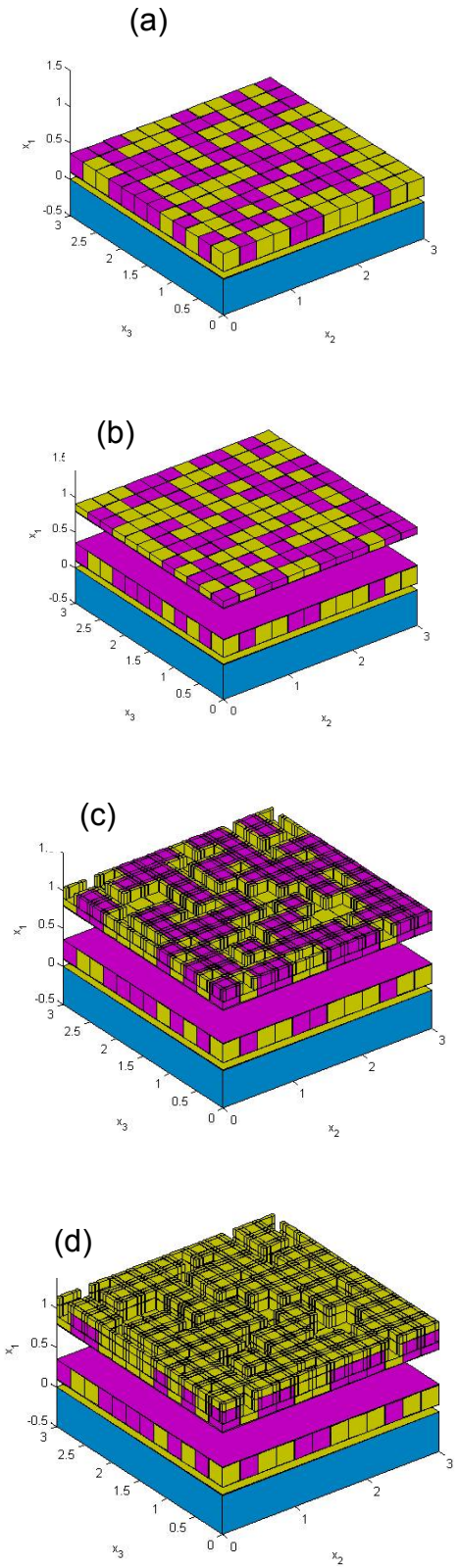

Fig. 2. Illustration of (a) initial ZnO pattern (b) definition of ZnO coverage layer (c) sidewall definition and (d) ZnO topmost coverage.

The definition of the sixth layer is a complicated process. In general each binary mask is divided into 9 sub-regions as illustrated in Fig. 1. For region surrounding the boundary, the refractive index can actually be ZnO, silicon, or air refractive index. In the case that the adjacent region is silicon, then the refractive index of these sub-regions should be ZnO since they consist of the sidewall of the strucuture. In the case that the underlying layer, i.e. the silicon/ZnO bottom grating layer is ZnO, then these sub-regions should be filled with silicon and thus silicon refractive index is used. In the case that the bottom silicon/ZnO grating is silicon, then then these sub-regions should be filled with air and thus air refractive index is used. The algorithm can be understood by referring to Fig. 1, the 9 subdivision is used to separately define the sidewall coverage. For the sub-region a,b,c,d,f,g,h,i, if the initial binary mask is 1, then silicon refractive index is used, and if one of the adjacent regions is silicon, then the ZnO refractive index is used. For remaining situations, the air refractive index is used.

For the sub-region at the center, i.e. sub-region e in Fig. 1, if the bottom silicon/ZnO grating is silicon, then then this sub-region should be filled with air and thus air refractive index is used. In the case that the bottom silicon/ZnO grating is ZnO, then then this sub-region should be filled with silicon for conformal coverage is assumed here and the silicon layer thickness is kept the same through the entire device.

III. Spectral Response and Transmission

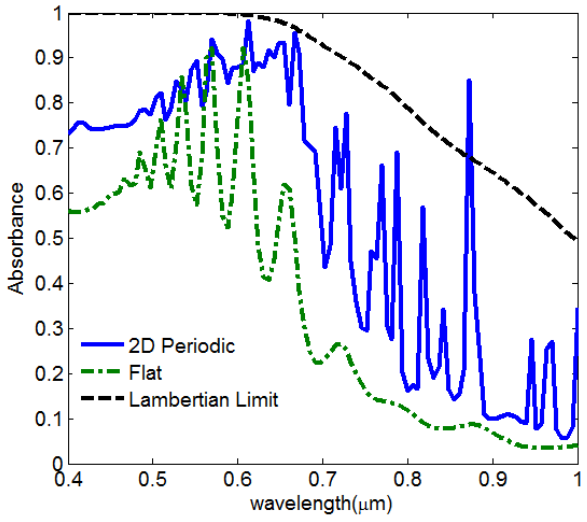

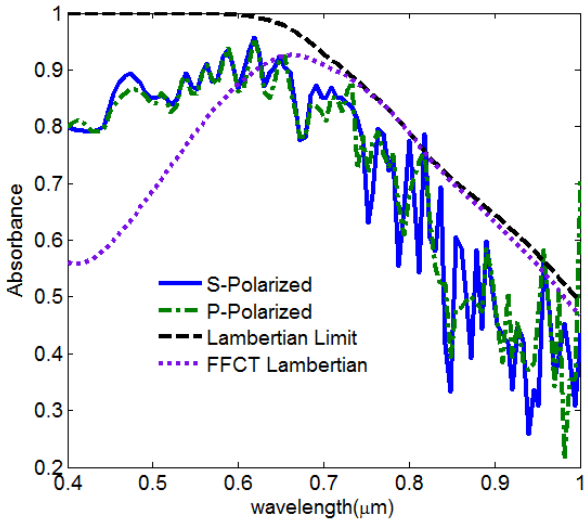

Fig. 3. Spectral responses for (a) 2D periodic grating (b) GA optimized quasi 4X4 random grating

Calculation of poynting vector, energy loss, and integrated quantum efficiency can be referred to literatures[2, 11, 22, 23]. A 4X4 quasi-random grating provides 23% broad band improvement reference to 2D periodic grating. At short wavelength, Genetic-Algorithm(GA)-optimized structures show broad band improvement due to transmission enhancement, as will be clear in Fig. 4. At long wavelengths, Fabry-Perot type resonance is seen in 2D-periodic grating due to quasi-guided mode excitation.

The Lambertian absorption limit is[24]:

$$A(\lambda) = \frac{(1-e^{-4\alpha W})}{[1-(1-1/n^2)e^{-4\alpha W}]} \qquad (1)$$

where α is absorption coefficient, n is semiconductor refractive index, and W is film thickness. Although at resonance frequency the absorption can exceed Lambertian limit for 2D periodic grating, the broad band enhancement is not as strong as GA-optimized structures. In the derivation of Lambertian limit in (1), the transmission at front surface is assumed to be unity and the front contact corrected transmission(FFCT) Lambertian limit in Fig. 3 takes into account the imperfect transmission at Air/ZnO/Silicon interface. Although at the resonance frequencies the absorbance of 2D periodic grating cell can exceed Lambertian limit, the broad band enhancement is not as strong as GA-optimized structures. This is due to the well-defined quasi-guided-modes in 2D periodic structures and thus pronounced absorption peaks are observed in spectral response. Nonetheless, at frequencies other than resonance, the absorption is much lower. Since it is difficult for guided mode to exist over entire solar spectrum for a particular incidence angle, a comprised but optimized random gratings provides higher overall efficiencies. Planar cell in general shows impedance matching characteristics at short wavelength where peaked absorbance is seen when wave impedance is matched through the solar cell stacks. It shows weak absorption at long wavelength due to insufficient light scattering, resulting from lack of large angle diffraction.

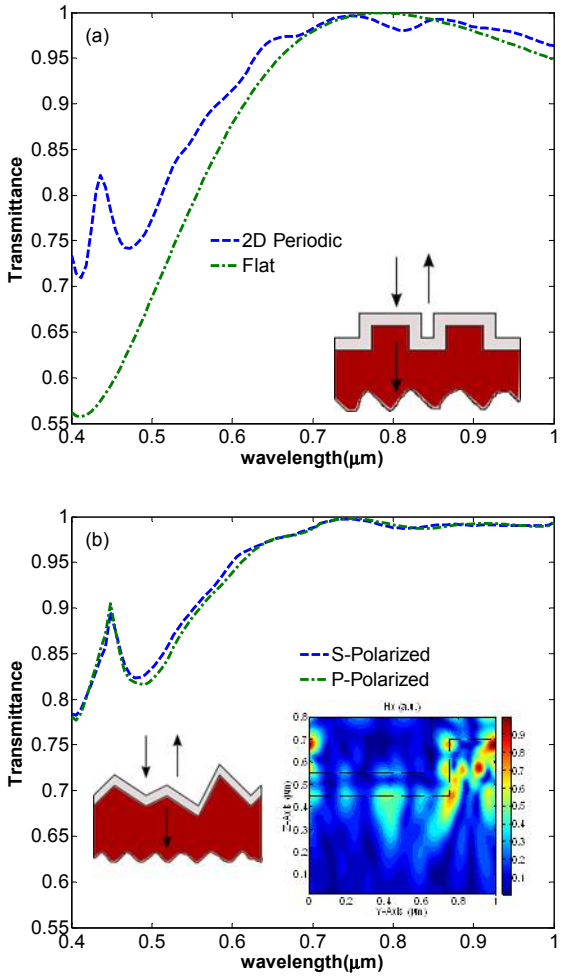

Fig. 4. Transmission for (a) 2D grating (b) GA optimized quasi 4X4 random grating (insect) p-polarized Hx field at transmission peak at λ= 448.5nm.

At long wavelength portion of the solar spectrum, the transmission is essentially very high due to impedance matched nature. The impedance matched condition for ZnO front contact assuming planar structure is:

$$t_{ZnO} = \frac{\lambda}{4n_{ZnO}} + \frac{m\lambda}{2n_{ZnO}} \qquad (2)$$

where λ is free space wavelength, n_{ZnO} is ZnO refractive index, and m is non-negative integer. For 2D-perioidic grating the transmission is further improved at all wavelengths where a broad band transmission is observed instead of a perfect transmission at a single wavelength, as is the case of planar

structure. The lower transmission at short wavelength for both Fig. 4 (a)(b) is due to two factors. First is directly from (2). n_{ZnO} is approximately equal to 2 and t_{ZnO} =100nm, the first impedance matched point is around λ=800nm, and the second is λ=266.67 nm. Since there is no impedance matched point around λ=400nm-600nm, the transmission is lower at short wavelength. The second reason is that the imaginary part of dielectric constant (ε_r") becomes higher at short wavelength, which in turn lowers the transmission. The transmission peak around λ=448.5nm is unlikely the result of impedance matching since there is no such points in this spectral range. It is more likely due to strong waveguiding effect where the ridged-geometry guides the incident wave into silicon slab as illustrated in the insect of Fig. 4(b). The further broad band transmission improvement of random grating over 2D periodic grating is due to optimized geometry by GA.

IV. Field Profile and Waveguiding Effect

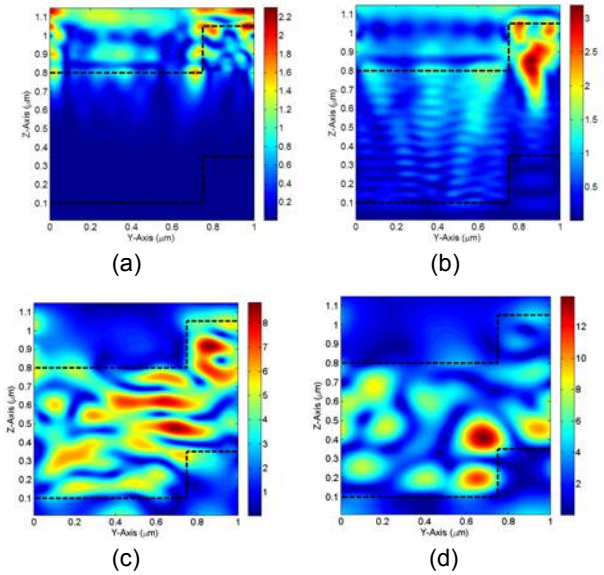

Fig. 5. P-polarized Hy field at (a)λ=400 nm (b)λ=473 nm (c)λ= 818nm (d)λ= 958nm at x=0.1μm for GA- optimized random grating.

In Fig. 5 small penetrating depth is observed At short wavelength. At λ= 472.7nm, the absorption peak is due to the Fabry-Perot type resonance, where pronounced layered field profile is the evidence of coupling into guided resonant mode. From 600nm-1000nm, broad band waveguiding effect is observed, where the incident wave is guided by the geometry of the grating structure into the silicon slab. It can be seen from Fig. 5 that the normally incident wave is obliquely penetrating into the silicon slab, which is the evidence of strong waveguiding effect. Since the quasi-guided mode is impossible to exist over entire spectral range, the randomized grating is a compromised solution over the entire spectrum and genetic algorithm is the way to find the integrated absorption peak. The s- and p- polarized spectral response shows similar absorptance due to the randomized nature. The polarization independent behavior is desired for solar cell application.

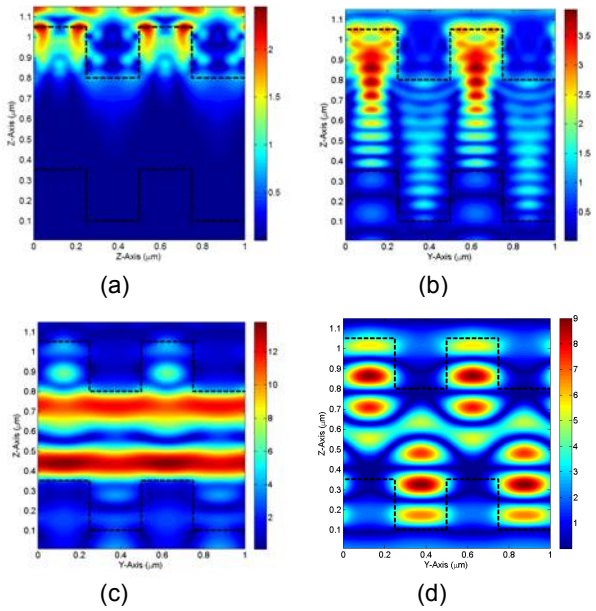

Fig. 6. P-polarized Hy field at (a)λ=400 nm (b)λ=515 nm (c)λ=818 nm (d)λ=921 nm at x=0.1μm for 2D Periodic grating.

In Fig. 6 the field profiles for 2D gratings is shown for comparison. Small penetration depth is also observed at short wavelength. From Fig. 4, the transmission is lower for 2D periodic grating, and thus its short wavelength absorption is not as high as randomized gratings. The Fabry-Perot resonance is observed at λ= 0.8182 m, where the quasi-guided mode is excited and the strong absorption peak exceeding corresponding Lambertian limit is observed by spectral response (Fig. 3(a)). Although the strong quasi-guided mode peak can be excited, the broad band enhancement is not comparable to optimized random reflector since broad band waveguiding is not as pronounced. Besides, the field profiles mostly preserve their normally incidence feature, and on the contrary for random grating, the waveguiding makes the normally incident wave obliquely penetrate the silicon slab, which in turn facilitate total internal reflection.

VI. Conclusion

Genetic Algorithm is effective in optimization of random reflector for solar cell application. The resulting geometry shows broad band field enhancement in both short and long wavelength region of solar spectrum. The enhancement in GA-optimized structure is due to broad band transmission at short wavelength and excitation of quasi-guided mode at long

wavelength. The encoding and evolutionary scheme presented here can be applied to large scale fully optimized structure where the resulting light trapping capability can exceed randomly textured Lambertian limit due to the optimized geometry specifically w.r.t. solar spectrum, in contrast to the isotropic and randomness nature of Lambertian surface. The practicability of large scale fully optimized binary random grating is evaluated. It is pointed out that infinitely large mask is unnecessary and the practical dimension of random mask should only have to be large enough to make fringing effect negligible.

ACKNOWLEDGEMENT

We acknowledge the support of high speed computing facilities from National Center of High-Performance Computing (NCHC), Hsinchu, Taiwan. The work is funded by National Science Council (NSC), Taiwan.

REFERENCES

[1] E. Yablonovitch, "Statistical Ray Optics," *J. Opt. Soc. Am.,* vol. 72, pp. 899-907, 1982.

[2] P. Bhattacharya, *Semiconductor Optoelectronic Devices, 2nd ed.* Upper Saddle River, NJ: Prentice-Hall, 2006.

[3] S. S. Hegedus and R. Kaplan, "Analysis of quantum efficiency and optical enhancement in amorphous Si p–i–n solar cells," *Prog. Photovolt. Res. Appl. ,* vol. 10, pp. 257–269 2002.

[4] J. Krc*, et al.*, "Potential of light trapping in microcrystalline silicon solar cells with textured substrates," *Prog. Photovolt. Res. Appl.,* vol. 11, pp. 429–436, 2003.

[5] C. Munuera*, et al.*, "Morphology of ZnO grown by MOCVD on sapphire substrates," *J. Cryst. Growth,* vol. 264, pp. 70-78, 2004.

[6] H. Sai*, et al.*, "Light trapping effect of submicron surface textures in crystalline Si Solar Cells," *Prog. Photovolt. Res. Appl.,* vol. 15, pp. 415–423, 2007.

[7] A. Shah*, et al.*, "Photovoltaic technology: the case for thin-film solar cells," *Science,* vol. 285, pp. 692-698, 1999.

[8] V. Shah*, et al.*, "Thin-film silicon solar cell technology," *Prog. Photovolt. Res. Appl. ,* vol. 12, pp. 113–142 2004.

[9] H. Stiebig*, et al.*, "Light trapping in thin-film silicon solar cells by nano-textured interfaces," in *SPIE*, 2006, pp. 619701-1–619701-9.

[10] M. A. Green*, et al.*, "Solar cell efficiency tables (Version 29)," *Prog. Photovolt. Res. Appl.,* vol. 15, pp. 35 –40, 2007.

[11] A. Lin and J. D. Phillips, "Optimization of random diffraction gratings in thin-film solar cells using genetic algorithms," *Solar Energy Materials and Solar Cells,* vol. 92, pp. 1689-1696, 2008.

[12] X. Sheng*, et al.*, "Optimization-based design of surface textures for thin-film Si solar cells," *Optics Express,* vol. 19, pp. A841-A850, 2011.

[13] J. M. Khoshman and M. E. Kordesch, "Optical constants and band edge of amorphous zinc oxide thin films," *Thin Solid Films* vol. 515, pp. 7393–7399, 2007.

[14] S. J. Kang and Y. H. Joung, "Influence of substrate temperature on the optical and piezoelectric properties of ZnO thin films deposited by rf magnetron sputtering," *Appl. Surf. Sci. ,* vol. 253, pp. 7330–7335, 2007.

[15] A. S. Ferlauto*, et al.*, "Analytical model for the optical functions of amorphous semiconductors and its applications for thin film solar cells," *Thin Solid Films* vol. 455 –456 pp. 388–392, 2004.

[16] O. S. O. A. (Author) and M. B. (Editor), *Handbook of Optics, Vol. 2: Devices, Measurements, and Properties, Second Edition* vol. 2: McGraw-Hill Professional, 1994.

[17] B. Deken*, et al.*, "Minimization of field enhancement in multilayer capacitors," *Computational Mater. Sci. ,* vol. 37, pp. 401–409, 2006.

[18] C. Henry, "Limiting efficiencies of ideal single and multiple energy gap terrestrial solar cells " *J. Appl. Phys. ,* vol. 51, p. 4494, 1980.

[19] H. Lipson and J. B. Pollack, "Automatic design and manufacture of robotic lifeforms," *Nature,* vol. 406, pp. 974-977, 2000.

[20] S. Preblea*, et al.*, "Two-dimensional photonic crystals designed by evolutionary algorithms," *Appl. Phys. Lett.,* vol. 86, pp. 061111-1-061111-3, 2005.

[21] L. Shen*, et al.*, "Design of two-dimensional photonic crystals with large absolute band gaps using a genetic algorithm," *Phy s. Rev. B,* vol. 68, pp. 035109-1-035109-5, 2003.

[22] C. AB, *Comsol Multiphysics RF Module User Guide V 3.3*, 2006.

[23] Synopsys, "Sentaurus Device EMW User Manual V. X-2005.10," ed, 2005, pp. 78-79.

[24] M. A. Green, "Lambertian Light Trappingin Textured Solar Cells and Light-Emitting Diodes: Analytical Solutions," *Prog. Photovolt: Res. Appl.,* vol. 10, pp. 235-241, 2002.

國科會補助計畫衍生研發成果推廣資料表

日期:2013/08/21

國科會補助計畫	計畫名稱: 以光場增強效應提升薄膜太陽能電池吸收效率研究
	計畫主持人: 林詩淳
	計畫編號: 101-2218-E-009-001- 學門領域: 太陽能光電

無研發成果推廣資料

101 年度專題研究計畫研究成果彙整表

計畫主持人：林詩淳	計畫編號：101-2218-E-009-001-
計畫名稱：以光場增強效應提升薄膜太陽能電池吸收效率研究	

成果項目			量化			單位	備註（質化說明：如數個計畫共同成果、成果列為該期刊之封面故事...等）
			實際已達成數（被接受或已發表）	預期總達成數(含實際已達成數)	本計畫實際貢獻百分比		
國內	論文著作	期刊論文	0	0	100%	篇	
		研究報告/技術報告	0	0	100%		
		研討會論文	0	0	100%		
		專書	0	0	100%		
	專利	申請中件數	0	0	100%	件	
		已獲得件數	0	0	100%		
	技術移轉	件數	0	0	100%	件	
		權利金	0	0	100%	千元	
	參與計畫人力（本國籍）	碩士生	4	4	100%	人次	
		博士生	2	2	100%		
		博士後研究員	0	0	100%		
		專任助理	0	0	100%		
國外	論文著作	期刊論文	3	3	100%	篇	The research results have been published in high quality journals including Optics Expres, Journal of Applied Physics.
		研究報告/技術報告	0	0	100%		
		研討會論文	3	3	100%		
		專書	0	0	100%	章/本	
	專利	申請中件數	0	0	100%	件	
		已獲得件數	0	0	100%		
	技術移轉	件數	0	0	100%	件	
		權利金	0	0	100%	千元	
	參與計畫人力（外國籍）	碩士生	0	0	100%	人次	
		博士生	0	0	100%		
		博士後研究員	0	0	100%		
		專任助理	0	0	100%		

其他成果 (無法以量化表達之成果如辦理學術活動、獲得獎項、重要國際合作、研究成果國際影響力及其他協助產業技術發展之具體效益事項等，請以文字敘述填列。)	無

	成果項目	量化	名稱或內容性質簡述
科教處計畫加填項目	測驗工具(含質性與量性)	0	
	課程/模組	0	
	電腦及網路系統或工具	0	
	教材	0	
	舉辦之活動/競賽	0	
	研討會/工作坊	0	
	電子報、網站	0	
	計畫成果推廣之參與（閱聽）人數	0	

國科會補助專題研究計畫成果報告自評表

請就研究內容與原計畫相符程度、達成預期目標情況、研究成果之學術或應用價值（簡要敘述成果所代表之意義、價值、影響或進一步發展之可能性）、是否適合在學術期刊發表或申請專利、主要發現或其他有關價值等，作一綜合評估。

1. 請就研究內容與原計畫相符程度、達成預期目標情況作一綜合評估

■達成目標

□未達成目標（請說明，以 100 字為限）

□實驗失敗

□因故實驗中斷

□其他原因

說明：

2. 研究成果在學術期刊發表或申請專利等情形：

論文：■已發表 □未發表之文稿 □撰寫中 □無

專利：□已獲得 □申請中 ■無

技轉：□已技轉 □洽談中 ■無

其他：(以 100 字為限)

3. 請依學術成就、技術創新、社會影響等方面，評估研究成果之學術或應用價值（簡要敘述成果所代表之意義、價值、影響或進一步發展之可能性）(以 500 字為限)

這一次的計畫在以下四方面有所貢獻：

1. 展示電磁模擬和奈米光學數值方法，是合適用在下一代太陽能電池的研究上。

2. 透過電磁模擬來達到太陽能電池之最佳設計和效率提升。

3. 對於電磁模擬、太陽能電池基礎光學和數值方法有更深入之研究，藉由光子能帶結構，反射透射吸收頻譜，繞射級數，以及波特徵模式的計算，得到設計上的想法。

4. 新式前瞻性的光學共振腔結構，以及其他具展望的光學結構，在這一次的計畫中被仔細討論檢視。相關的提議(proposal)，將透過光子能帶結構，反射透射吸收頻譜 以及波特徵模式的計算，對一下代太陽能電池產生貢獻。